# Designing a robust whole-cell biosensor for detection of toxic metals using intein splicing inhibition of *Mycobacterium tuberculosis* SufB protein

Ashwaria Mehra[1†], Ananya Nanda[1,2†], and Sasmita Nayak[1, 3#]

[1] School of Biotechnology, Kalinga Institute of Industrial Technology Deemed to be University, Bhubaneswar, Odisha, India 751024.
[2]Toronto Metropolitan University, 350 Victoria St, Toronto, ON M5B 2K3, Canada
[3] Department of Microbiology, Kalinga Institute of Medical Sciences, Kalinga Institute of Industrial Technology Deemed to be University, Bhubaneswar, Odisha, India 751024

[#]Corresponding Author: sasmita.n@kiitbiotech.ac.in

[†]These authors have contributed equally to this work and share first authorship

**Running Title:** Intein-based whole-cell biosensor detects toxic metals

**Abbreviation:**

Ni-NTA: Nickel-nitrilotriacetic acid

TCEP.HCl: Tris 2-carboxyl ethyl phosphine. Hydrochloric acid

IPTG: Isopropyl β-d-1-thiogalactopyranoside

Trp: Tryptophan

SDS: Sodium Dodecyl Sulfate

PAGE: Polyacrylamide gel electrophoresis

ICP-OES: Inductively Coupled Plasma Optical Emission Spectroscopy

UV-Vis: UV-visible spectroscopy

PVDF: Polyvinylidene fluoride

BSA: Bovine serum albumin

28 *Mtb*: *Mycobacterium tuberculosis*

29 WT: Wild type

30 SI: Splicing inactive

31 $Cd^{2+}$: Cadmium

32 $Hg^{2+}$: Mercury

33 $Pb^{2+}$: Lead

34 $Cr^{3+}$: Chromium

35 $Cu^{2+}$: Copper

36 $Zn^{2+}$: Zinc

37 $Pt^{4+}$: Platinum

38

39 **Abstract**

40 Disruption of the natural geochemical cycle by human activities has led to bioaccumulation of
41 metals, posing a global health threat. Hence, there is a pressing need for simple, sensitive, yet eco-
42 friendly biosensor setups to monitor metal contamination in the environment. Existing biosensors
43 are limited by poor efficiency, stability issues, and complex instrumentation requiring skilled
44 operators. To address these caveats, current study explores how intein-mediated protein splicing,
45 a spontaneous post-translational process, can be adapted for metal-biosensing by coupling metal-
46 dependent splicing inhibition to viability loss of native microbial cells. Toxic metal ions like $Cd^{2+}$
47 and $Hg^{2+}$ attenuated the splicing activity of *Mtb* SufB precursor protein over a concentration range
48 of 25 μM to 2 mM, while $Pb^{2+}$ and $Cr^{3+}$ failed to do so. An innovative biosensor platform was
49 designed for colorimetric detection of metal ions via simple Alamar Blue assay, where attenuated
50 *Mtb* strain (H37Ra) served as the indicator cells. Metal-induced SufB splicing inhibition led to loss
51 of viability of H37Ra cells, while addition of metal-specific chelators reversed the effect.

Multiplexing ability was evaluated by including known splicing inhibitors like $Cu^{2+}$, $Zn^{2+}$, and $Pt^{4+}$ over various concentration range alongside $Cd^{2+}$ and $Hg^{2+}$. The simple 96-well plate format enables multiplexed qualitative metal detection, while colorimetric absorbance measurement ensures metal quantification. The designed biosensor offers low-cost, user-friendly, and sensitive assay for high-throughput metal detection, utilizing whole-cell native organisms carrying metal-sensing precursor protein. Thus, this approach can be implemented in standard biological laboratories for robust metal screening process in environmental and industrial effluents.

**Keywords:** Whole-cell biosensor, heavy metal ion detection, *Mycobacterium tuberculosis* SufB, intein-based biosensor, protein splicing inhibition.

## Introduction

Heavy metal contamination has emerged as one of the most persistent environmental and public health challenges of the modern era. Over 35 metals have been identified in their ore forms within the Earth's crust, many of which are essential nutrients. Among these, 23 metals are classified as heavy metals due to their high density (>5 g/cm³) and atomic weights (>40.0), indicating their potential for environmental toxicity (1–3). Human activities have significantly disrupted natural geochemical cycles, causing bioaccumulation and biomagnification through contaminated food, water, or direct exposure, thereby posing serious health risks (3–7).

Current analytical methods, such as electrothermal atomic absorption spectrometry (ETAAS), inductively coupled plasma-optical emission spectrometry (ICP-OES), high-pressure liquid chromatography combined with ICP-mass spectrometry (HPLC-ICP-MS), hydride generation atomic absorption spectrometry (HGAAS), and X-ray fluorescence spectrometry (XRF), offer excellent sensitivity for detecting metals. Nonetheless, these methods involve complex

instrumentation, require skilled operators, generate hazardous waste, contributing further to environmental pollution (8–11). To overcome these limitations, biosensors have emerged as a promising alternative offering affordability, and long-term operational stability (8). According to the International Union of Pure and Applied Chemistry (IUPAC), biosensors integrate biological recognition elements directly with transducers to provide precise quantitative data (12, 13). Although enzyme-based electrochemical biosensors have been widely explored, their broader implementation is limited due to poor electron transfer efficiency, and instability, limiting their commercial reusability (14–20). In comparison, whole-cell biosensors present a more practicable approach by using live cell sensing units, with advantages such as stable signal generation, and scalability. For instance, Chouteau et al. synthesized BSA encapsulated microalgae as bioreceptors to detect metals ($Cd^{2+}$, $Zn^{2+}$, and $Pb^{2+}$) (16). However, the sensitivity of detection was affected due to variability in algal loading and distribution within BSA membrane. In another work, transformed protozoan cells were used as whole-cell biosensor, linking the metallothionein promoter-based metal detection to luciferase reporter system (21). Despite the innovation, signal variability compromised the specificity and sensitivity of heavy metal detection. In another study, Kim and colleagues engineered *E. coli* cells carrying plasmids with metal sensing promoters to detect metals such as $Cu^{2+}$, $Zn^{2+}$, and $Cd^{2+}$ (22). However, the $Cu^{2+}$ and $Cd^{2+}$ sensing strains were not selective and could also detect other metals. Further, detection of $Cu^{2+}$ was hindered by the active transport of $Cu^{2+}$ ions out of the cytoplasm by the endogenous CopA protein, suppressing reporter gene expression. Other challenges with whole-cell biosensors include declining cell viability causing delayed response time, leaky gene expression inducing false positive signals, and ecological threats of using genetically modified organisms (23–29). Addressing these

96 shortcomings, intein-mediated protein engineering techniques open up new avenues for creating
97 innovative cell-based sensors (30–33).

98 Inteins are protein splicing elements within precursor proteins that can self-excise via multi-step
99 nucleophilic displacement reactions, to generate active proteins (Supplemental Fig. S1) (34, 35).
100 This is a post-translational process that does not require energy sources or cofactors, hence inteins
101 can be seamlessly integrated into biosensor units minimizing interference with sensor cell
102 functionality (30). Furthermore, intein splicing in precursor proteins can be regulated via
103 conditional protein splicing (CPS), in presence of small molecules such as metal ions and metal-
104 based nanoparticles (Table 1) (36–42). For instance, a recent study from our group has examined
105 the splicing and N-terminal cleavage activity of *Mycobacterium tuberculosis* (*Mtb*) SufB precursor
106 protein in the presence of metal ions such as $Cu^{2+}$, $Zn^{2+}$, $Pt^{4+}$, and $Fe^{3+}/Fe^{2+}$ (43). Prior studies
107 have also reported $Zn^{2+}$ mediated splicing regulation of PI-*Sce* VMA intein, *Mtb* RecA intein, and
108 *Ssp* PCC6803 DnaE split intein (44, 45). Effects of metal ions, such as $Cu^{+/2+}$ and CisPt, have been
109 evaluated on *Mtb* RecA, *Cryptococcus neoformans* Prp8, and *Mycobacterium smegmatis* DnaBi1
110 intein splicing (38, 39, 44, 46–51).

111

112

113

114

115

116 **Table 1:** Overview of intein-harboring organisms and reported modulation of splicing activity by
117 metal ions

118

| Organisms | | Intein containing precursor proteins | Metal ions | References |
|---|---|---|---|---|
| **Bacteria** | *Mycobacterium tuberculosis* | RecA | $Zn^{2+}$<br>$Cd^{2+}$<br>$Co^{2+}$<br>$Ni^{2+}$<br>$Cu^{+}/Cu^{2+}$<br>CisPt | (45, 47, 52, 53) |
| | *Mycobacterium tuberculosis* | SufB | $Zn^{2+}$<br>$Cu^{2+}$<br>$Pt^{4+}$<br>$Fe^{2+/3+}$ | (43) |
| | *Mycobacterium smegmatis* | DnaB-intein1 (DnaBi1) | $Zn^{2+}$ | (49) |
| | *Synechocystis* sp. PCC6803 | *Ssp* DnaE | $Zn^{2+}$<br>$Cd^{2+}$ | (45) |
| | *Oscillatoria limnetica* | split DnaE intein | $Cu^{2+}$ | (54) |
| | *Thermosynechococcus vulcanus* | DnaE | $Cu^{2+}$ | (54) |
| | *Nostoc* sp. PCC7120 | DnaB | $Cu^{2+}$ | (54) |
| **Fungi** | *Saccharomyces cerevisiae* | PI-*Sce*I VMA | $Zn^{2+}$ | (44) |
| | *Cryptococcus neoformans* | Prp8 | $Zn^{2+}$<br>$Cu^{2+}$<br>CisPt | (39, 51) |
| | *Cryptococcus gattii* | Prp8 | CisPt | (51) |

119

120

121 Conditional splicing activity of intein-containing proteins has been used to (30, 55–58) design
122 biosensors to detect protein~protein interaction in living cells via split GFP (52) or Luciferase
123 reporter system (53–55). Although several fundamental studies have reported splicing regulation
124 of precursor protein in presence of oxidative/nitrosative stresses (56), metal ions (43),
125 nanoparticles (40) correlating to pathogen survival, a versatile and native whole cell intein-based
126 biosensor, especially for toxic metal ion detection, is yet to be elucidated.

127 However, concerns pertaining to the functionality and usability of the intein-based metal-sensing
128 biosensor remains, such as: 1) If an eco-friendly whole cell biosensor system can be designed using
129 native cells without any genetic modification; 2) Whether the designed biosensor can offer an user-
130 friendly and low-cost approach?; 3) If the working protocol can be simple, yet effective for a
131 specific, and sensitive metal detection?; And finally, 4) Whether this approach can be applied for
132 a multiplexed metal screening process, for qualitative and quantitative detection of different metal
133 ions? Current research explores how toxic metal ions, like cadmium ($Cd^{2+}$), mercury ($Hg^{2+}$),
134 chromium ($Cr^{3+}$), and lead ($Pb^{2+}$), affect the splicing and N-terminal cleavage reactions of *Mtb*
135 SufB precursor protein. The fundamental knowledge gained from these results was applied to
136 develop a biosensor platform to detect toxic metals, using native mycobacterial cells in a 96-well
137 plate format. Splicing regulation in metal-sensitive precursor protein *Mtb* SufB induced alteration
138 in mycobacterial cell viability, that indicated the presence of metal ions.

139 *Mtb* SUF protein complex constitutes an unique pathway for Fe-S cluster assembly in
140 mycobacteria, and its activity is dependent on the splicing of SufB precursor, producing functional
141 SufB protein (60). Thus, splicing inhibition which blocks the generation of active SufB, can retard

142 mycobacterial growth and viability by impairing Fe-S cluster biogenesis (61). In the current work,
143 *in vitro* studies demonstrated significant inhibition of *Mtb* SufB precursor protein splicing in
144 presence of toxic metal ions such as $Cd^{2+}$, and $Hg^{2+}$ over a concentration range of 25 μM to 2 mM.
145 Further, time-dependent assay revealed that $Cd^{2+}$ and $Hg^{2+}$ inhibit *Mtb* SufB intein splicing as early
146 as 10 minutes following exposure to the metal ions. Building on this observation, a biosensor
147 platform was designed using native H37Ra (an attenuated *Mtb* strain) as the metal-indicator cells.
148 Alamar Blue assay performed in a 96-well microtiter plate, detected loss of cell viability in SufB-
149 containing H37Ra cells in presence of toxic metal ions, $Cd^{2+}$ and $Hg^{2+}$. In a control study,
150 *Mycobacterium smegmatis* (*M. sm*), which expresses an intein-less SufB protein, persisted as
151 healthy, viable cells under similar experimental conditions. These results highlight the sensitivity
152 of H37Ra-based biosensor platform to detect toxic metal ions over a concentration range of 25 μM
153 to 2 mM. The specificity of the designed biosensor was assessed by adding respective metal
154 chelators, which protected mycobacterial cell viability, by blocking the splicing-inhibitory activity
155 of metal ions. Moreover, multiplexing and quantitative potential of the biosensor platform was
156 validated by using various concentrations of known splicing inhibitors [$Zn^{2+}$, $Cu^{2+}$, and $Pt^{4+}$ (43)]
157 alongside $Cd^{2+}$ and $Hg^{2+}$. The high throughput design enables simultaneous testing of many
158 samples for a qualitative metal detection, while absorbance measurement from the colorimetric
159 Alamar Blue Assay ensures metal quantification extrapolated to a standard plot. Thus, this work
160 opens new avenues for developing a reliable and sensitive biosensor platform using whole-cell
161 mycobacteria as biological indicator for toxic metal ions as well as trace metal elements (TME) in
162 the environmental samples. The efficacy of this system lies in its user-friendly design, specificity,
163 and sensitivity, enabling multiplexed metal detection by non-genetically modified whole cell
164 microbes. Consequently, the working principle can be easily optimised and employed in standard

165 biological laboratories equipped with organisms harboring other metal-sensitive intein-carrying
166 precursor proteins.

167 **Experimental Procedure:**

168 *Experimental Design and Statistical Rationale*

169 Current study was designed to evaluate intein splicing-based whole-cell mycobacterial biosensor,
170 where splicing inhibition in the metal-sensing SufB precursor protein, reduced mycobacterial
171 viability. During *in vitro* refolding assay, purified denatured *Mtb* SufB precursor and *Mtb* SufB
172 splicing inactive (SI) double mutant (Cys1Ala/Asn359Ala) (splicing negative control) proteins
173 were renatured in the absence and presence of $CdCl_2$, $HgCl_2$, $CrCl_3$, and $PbCl_2$ over the test
174 concentration range (2.5 µM–2 mM). All the experiments were performed in triplicates (n=3) and
175 the protein products from the Coomassie-stained SDS–PAGE gels were quantified by
176 densitometric analysis using GelQuant.NET biochemical solutions software. The splicing and
177 cleavage efficiencies were calculated and expressed as percentage values after baseline correction,
178 using 0 hour splicing and cleavage value(s).

179 For evaluation of the metal biosensor, a simple Alamar Blue assay was conducted, where different
180 mycobacterial cells [*Mtb* H37Ra cells and *Mycobacterium smegmatis* (SufB intein-less)] were
181 incubated with varied concentrations of $Cd^{2+}$ (2.5 µM- 2 mM) and $Hg^{2+}$ (25 µM- 2 mM) in 96-
182 well microtiter plate. In a parallel experimental setup, $Cd^{2+}$ and $Hg^{2+}$ specific metal chelators were
183 added in a ratio of 1:1 (metal: chelator) to examine the specificity of the biosensor platform. For a
184 quantitative evaluation, standard plots were generated by correlating the known concentrations of
185 samples [$Cd^{2+}$ and $Hg^{2+}$] along the X-axis, to the respective absorbance values from the Alamar
186 Blue assay on the Y-axis. Test metal concentrations in the unknown samples were interpolated

187 from the standard curve to validate the biosensor efficacy. Multiplexing ability of the whole -cell
188 biosensor was assessed using known splicing inhibitors $ZnCl_2$, $CuCl_2$, and $PtCl_4$, along with $CdCl_2$
189 and $HgCl_2$, under identical experimental conditions.

190 Statistical analysis for refolding assays was performed using one-way analysis of variance
191 (ANOVA) to compare splicing and N-terminal cleavage efficiencies of metal treated samples
192 against the untreated protein control, after baseline correction using 0 h values, and results were
193 plotted using GraphPad Prism version 5.01 for Windows, GraphPad Software, SanDiego, CA,
194 U.S.A. (www.graphpad.com). The data are presented as mean ± SEM. The statistical significance
195 (p-value) between the control and experimental groups is denoted by * ($p < 0.05$), or ** ($p < 0.01$),
196 or *** ($p < 0.001$), or ****($p<0.0001$).

197 *Protein overexpression and purification* (62–64)

198 Plasmids containing the genes for *Mtb* SufB precursor and *Mtb* SufB splicing inactive (SI) double
199 mutant (Cys1Ala/Asn359Ala) (splicing negative control), both carrying an N-terminal 6X (His)
200 tag, were borrowed from Belfort Lab, SUNY, Albany, USA)(62). The test plasmids were
201 transformed into BL21(DE3) *E. coli* cells (NEB, C2527I), followed by IPTG (500 µM, sigma 367-
202 93-1) induced protein over-expression. Thereafter, lysis buffer (20 mM sodium phosphate, 0.5 M
203 NaCl, pH 7.4) was used to resuspend the bacterial cell pellet and cells were lysed via tip sonicator
204 (Sonics vibra cell VCX-130). The cell lysate was centrifuged at 16500×g for 20 minutes at 4 °C,
205 and the supernatant was discarded. The collected inclusion body (IB) material was then washed
206 three times in lysis buffer via centrifugation (16500×g for 20 minutes at 4 °C). Finally, the IB
207 material was solubilized for protein extraction using 8 M urea (Merck, 1084870500) buffer (20
208 mM sodium phosphate, 0.5 M NaCl, 8M urea, 10 mM of imidazole, pH 7.4 (MP–biochemicals-

209 288-32-4) and subsequently centrifuged at 16,500×g for 20 minutes at 4 °C to collect the
210 supernatant. Then, solubilized proteins were purified by Ni-NTA affinity column (Ni-NTA His
211 trap, HP GE healthcare life sciences, 17524802) (38, 45, 58, 65, 66). Before applying the samples,
212 the columns were equilibrated with binding buffer (20 mM sodium phosphate, 0.5 M NaCl, 8 M
213 urea, 10 mM imidazole, pH 7.4). Following sample loading, the columns were washed multiple
214 times (5 CV) using wash buffer (20 mM sodium phosphate, 0.5 M NaCl, 8 M urea, 40 mM
215 imidazole, pH 7.4). Subsequently, the test proteins were eluted as purified fractions using elution
216 buffer (20 mM sodium phosphate, 0.5 M NaCl, 8 M urea, 500 mM imidazole, pH 7.4). Protein
217 quantification was performed using Bradford reagent.

218 *Refolding assay for Mtb SufB precursor protein*

219 Denatured protein (2.5 μM) in elution buffer was renatured in refolding buffer (20 mM sodium
220 phosphate, 0.5 M NaCl, 0.5 M L-Arginine) containing 2 mM TCEP-HCl (sigma-51805-45-9) for
221 4 hours at 25 ºC in the absence and presence of toxic metal ions (45, 65, 66). Gradient assay for
222 toxic metal ions [$CdCl_2$ (SRL-99643), $HgCl_2$ (SRL-25699), $CrCl_3$ (CDH-025702), $PbCl_2$ (SRL-
223 69789)] was performed using varying concentrations of toxic metal ions (2.5 μM to 2 mM). 0h
224 sample was collected before initiation of refolding, and the reaction was abruptly blocked by the
225 addition of loading dye (0.1% bromophenol blue, 50% glycerol, 5% β-mercaptoethanol, 10% SDS,
226 tris 6.8), followed by rapid freezing at −20 ºC. After 4h of protein renaturation, the protein samples
227 were resolved through 4~10% gradient SDS-PAGE, followed by staining with Coomassie brilliant
228 blue R-250 (93473, SRL), and densitometric analysis was performed using GelQuant.NET
229 biochemical solutions software. The splicing and cleavage efficiencies were calculated using the
230 following formulae:

231 $$\% \, of \; splicing = \frac{Total \; splicing \; products \; (LE + I)}{Total \; protein \; (P + LE + I)} \; X \; 100$$

232 $$\% \, of \; N - terminal \; cleavage = \frac{Total \; N - terminal \; cleavage \; products \; (NC + NE)}{Total \; protein \; (P + NC + NE)} \text{X } 100$$

233 [P: precursor protein, LE: Ligated exteins, I: Intein, NC: N-terminal cleavage product, NE: N-
234 extein]

235 Baseline correction was done using the 0 hours splicing and cleavage value(s). The results were
236 analyzed using one-way ANOVA and plotted using GraphPad Prism version 8 for Windows,
237 GraphPad Software, San Diego, California, USA, www.graphpad.com.

238 *Immunoblotting to identify splicing and N-terminal cleavage protein products*(43)

239 Protein immunodetection was conducted to identify of splicing and N-terminal cleavage reaction
240 products, using anti-6X(His) tag antibodies (Invitrogen, LOT 1902132). After resolution through
241 4~10% gradient SDS-PAGE, the protein products were transferred onto a PVDF membrane
242 (Millipore, IPVH 00010) at 50V for 2 hours at 4 °C. The blot was then blocked with 5% skim milk
243 for 2 hours at room temperature, followed by two washes with 1X TBST. It was incubated with
244 primary anti-6X(His) tag (abgenex -32-6116) at a dilution of 1:5000 at 4 °C for 16 hours. After
245 washing with 1X TBST, the blot was treated with a secondary antibody (anti-mouse; abgenex 11-
246 301) at a dilution of 1:8000 for 2 hours at 37 °C. The N-extein band was detected using a lower
247 dilution of the primary antibody (1:2500) and the secondary antibody (1:6000). Finally, the blot
248 was developed using Enhanced Chemiluminescence substrate (Abcam, ab65628) to visualize the
249 protein bands, and images were captured using in-house ImageQuant™ LAS 500 facility (GE
250 Healthcare). Blots were also developed, using 3, 3'-diaminobenzidine (DAB) (SRL-94524) for
251 visualization of the protein bands.

252 *Spectroscopic and Elemental Profiling of Protein-Metal Interactions*

253 *UV-Visible spectroscopy* (67–69)

254 Denatured proteins were renatured *in vitro* in the presence and absence of toxic metal ions at their
255 respective concentrations for 4 hours, as specified earlier. Subsequently, the treated samples were
256 subjected to UV-visible spectroscopy (Cary 100 UV-Vis Agilent Technology) scanning in the
257 visible region spanning 200-800nm. To rule out the interference from buffer-metal interactions,
258 the refolding buffer (20 mM sodium phosphate, 0.5 M NaCl, 0.5 M L-Arginine) was incubated
259 with metal ions ($Cd^{2+}$, $Hg^{2+}$, $Cr^{3+}$, and $Pb^{2+}$) at their respective concentrations under similar
260 experimental conditions. This was used as a blank for baseline correction and was scanned
261 alongside each sample. Absorbance versus wavelength plots were generated and analyzed using
262 Origin (Pro) 8.5 software (Version 8.5, OriginLab Corporation, Northampton, MA, USA) to
263 interpret the results.

264 *Tryptophan Fluorescence Spectroscopy*

265 The purified denatured protein (2.5 μM) was allowed to renature in the presence and absence of
266 metals ions (25 μM $CdCl_2$, 500 μM $HgCl_2$, 2 mM $CrCl_3$, and 2 mM $PbCl_2$) under identical
267 experimental conditions. Following 4 hours of refolding, the test samples were analyzed via
268 Fluorescence spectrometry (Cary Eclipse, Agilent Technologies) over a wavelength range of 300-
269 600 nm and at an excitation wavelength of 280 nm (70). To rule out the buffer-metal interactions,
270 the refolding buffer (20 mM sodium phosphate, 0.5 M NaCl, 0.5 M Arginine) was incubated with
271 metal ions at their respective concentrations at 25 °C for 4 hours and then scanned alongside each
272 treated sample. This served as the blank for baseline correction. The tryptophan fluorescence
273 spectra for the test samples were recorded and analyzed by plotting intensity vs. wavelength using
274 Origin (Pro) 8.5, Version 8.5, from OriginLab Corporation, Northampton, MA, USA.

275 *Inductively coupled plasma-optical emission spectroscopy (ICP-OES) analysis*

276 Following *in vitro* refolding of *Mtb* SufB precursor in the presence of test metal ions, the protein
277 products were resolved through 4~10% SDS-PAGE. The resulting protein bands were visualized
278 with Coomassie brilliant blue R-250. Subsequently, the gel bands for unspliced precursor protein,
279 ligated extein, and intein were excised from the gel for further analysis. Each gel band was then
280 treated with concentrated $H_2SO_4$ and 30% $H_2O_2$. Complete dissolution of each sample was
281 achieved by incubating the gel pieces in a 3:1 mixture of concentrated HCl and concentrated $HNO_3$
282 at 80°C for 4 hours (71, 72). The final volume of the digested solution was adjusted to 50 ml with
283 deionized water and then analyzed by ICP-OES (Perkin-Elner, optima 8300). Prior to analyzing
284 the test samples, respective toxic metal standards were calibrated in the system, and the
285 concentration of bound metal ions was quantified from the standard curve.

286 *H37Ra-based whole-cell toxic metal biosensor*

287 Different mycobacterial cells [*Mycobacterium tuberculosis* H37Ra strain (ATCC 25177),
288 *Mycobacterium smegmatis* (negative control for SufB intein-less micro-organism, ATCC
289 700084)] were cultured in 7H9 (Middlebrook 7H9 broth medium, M198) supplemented with
290 OADC (Oleic acid, dextrose, and catalase, Himedia-FD018) and allowed to grow separately for 2-
291 3 weeks at 37 $^0$C. CFU calculations for individual cultures were made by matching the turbidity
292 of the inoculated mycobacterial culture with the McFarland standard (Himedia- R092) against a
293 black background (73). Different bacterial cells were diluted in sterile saline to a concentration of
294 $10^8$ CFU/ml. H37Ra cells were incubated with varied concentrations of $Cd^{2+}$ (2.5 µM- 2 mM) and
295 $Hg^{2+}$ (25 µM- 2 mM) in 96-well microtiter plate. Since $Cr^{3+}$ and $Pb^{2+}$ over a test concentration
296 range of 25 µM- 2 mM did not exert any effect on *Mtb* SufB splicing, these metal ions were not
297 tested via the designed biosensor platform. The plates were sealed and incubated at 37 ºC for 4

298 days. Then, 10% (v/v) solution of Alamar Blue reagent (SRL-42650) was added to each well,
299 followed by incubation at 37 ºC for 12 hrs.(74). Untreated mycobacterial cells grown in 7H9
300 (supplemented with OADC) media were used as a negative control, and Alamar blue reagent alone
301 in 7H9 (supplemented with OADC) media served as a positive control. SufB intein-less organism,
302 *Mycobacterium smegmatis,* was also evaluated under similar conditions and treated as an
303 additional experimental control. After 12 hours of incubation, varied color changes were noted in
304 different wells, where blue color indicated dead cells with no viable cell growth, and pink color
305 correlated to metabolically active live cells. In a similar experimental setup, metal chelators
306 specific for $Cd^{2+}$ (Edetate Calcium Disodium, ECD, Sigma-PHR1510) and $Hg^{2+}$ (meso-2,3-
307 Dimercaptosuccinic acid, DMSA, Sigma-D7881) were added in a ratio of 1:1 (metal: chelator) to
308 determine the specificity of the designed Biosensor platform.

309 Quantitative evaluation of *H37Ra-based whole cell toxic metal biosensor*

310 Next, a standard plot was generated by measuring the absorbance of the respective samples at
311 570 nm, with 600 nm as a reference wavelength for quantitative analysis (74). A wide range of
312 test metal samples ($Cd^{2+}$, $Hg^{2+}$) of known concentration were prepared and loaded onto the 96-
313 well plate and Alamar Blue reagent was added under similar experimental conditions. The
314 absorbance of test metal samples was calculated by subtracting the reference absorbance value at
315 600nm from the absorbance measured at 570nm [$OD_{test} = OD_{570} - OD_{600}$]. Untreated mycobacterial
316 cells grown in 7H9 (supplemented with OADC) media were used as a control for normalization.
317 Using the normalized values, XY scattered plot was obtained where the X axis represented the
318 known concentrations of the test metal ions and the Y axis denoted corresponding absorbance
319 values. Next, to assess the applicability of the standard plot, four test samples (Unknown 1,
320 Unknown 2, Unknown 3, and Unknown 4) containing varying concentrations of $CdCl_2$ and $HgCl_2$

321 were analyzed under identical experimental conditions. Absorbance values were extrapolated onto
322 the standard curve to calculate the unknown metal ion concentrations, thereby validating the
323 sensitivity and accuracy of the biosensor platform.

324 *Multiplexing evaluation of H37Ra-based whole cell metal biosensor*

325 Bacterial cell suspension containing $10^8$ CFU/ml of *Mycobacterium tuberculosis* H37Ra were
326 prepared in sterile saline. Cells were incubated with a varied concentration range of $ZnCl_2$ (100
327 µM- 2 mM), $CuCl_2$ (100 µM- 2 mM), $PtCl_4$ (20 µM- 1 mM), $CdCl_2$ (10 µM- 2 mM), and $HgCl_2$
328 (25 µM- 2 mM), in 96-well microtiter plates. The plates were sealed and incubated at 37 ºC for 4
329 days under static conditions. Then, 10% (v/v) solution of Alamar Blue reagent (SRL-42650) was
330 added to each well, followed by incubation at 37 ºC for 12 hrs. Untreated H37Ra cells grown in
331 Middlebrook 7H9 supplemented with OADC media were used as a negative control, while Alamar
332 blue reagent incubated in media alone served as a positive control. SufB intein-less organism,
333 *Mycobacterium smegmatis,* was treated with test metal ions under similar conditions and used as
334 negative experimental control to assess SufB intein-specific response. Post 12 hours of incubation,
335 color change was noted in the wells, where blue color indicated dead cells with no viability, and
336 pink color indicated healthy viable cells.

337 To further ascertain the specificity of the biosensor platform, respective metal-chelating agents
338 were added in separate experimental setup, using a 1:1 molar ratio of metal ions to chelator.
339 Cadmium-specific chelator Edetate Calcium Disodium (ECD; Sigma-PHR1510), mercury-
340 specific chelator meso-2,3-Dimercaptosuccinic acid (DMSA; Sigma-D7881), and a broad-
341 spectrum chelator Ethylenediaminetetraacetic acid (EDTA; HiMedia-MB011), were co-incubated

342 with the respective metal ions under identical experimental conditions. Cell viability was evaluated
343 using Alamar Blue reagent as described earlier.

344 *Statistical Analysis*

345 Statistical analysis for refolding assays was performed using one-way analysis of variance
346 (ANOVA) to compare splicing and N-terminal cleavage efficiencies of metal treated samples
347 against the untreated protein control, after baseline correction using 0 h values, and results were
348 plotted using GraphPad Prism version 5.01 for Windows, GraphPad Software, SanDiego, CA,
349 U.S.A. (www.graphpad.com). The data are presented as mean ± SEM. The statistical significance
350 (p-value) between the control and experimental groups is denoted by * ($p < 0.05$), or ** ($p < 0.01$),
351 or *** ($p < 0.001$), or ****($p<0.0001$).

352 **Results and Discussion**

353 ***Toxic metal ions inhibited Mtb SufB precursor protein splicing***

354 Environmental concentrations of toxic metal ions such as cadmium ($Cd^{2+}$), mercury ($Hg^{2+}$),
355 chromium ($Cr^{3+}$) and lead ($Pb^{2+}$) have been reported to vary widely. $Cd^{2+}$ concentrations typically
356 ranges from 1 to 10 ppm (approximately 5 μM to 55 μM), $Hg^{2+}$ from 10 to 700 ppm
357 (approximately 4 μM to 3 mM), $Cr^{3+}$ from 5 ppm- 140 ppm (approximately 31 μM – 885 μM) and
358 $Pb^{2+}$ levels from 10 to 50 ppm (approximately 36 μM to 180 μM) (75–90). Earlier studies have
359 shown that metal ion concentrations between 40 μM to 2 mM effectively inhibit intein splicing
360 (43, 91, 92). Built upon these observation, *in vitro* gradient assay was performed to evaluate the
361 sensitivity of *Mtb* SufB precursor protein to a selected concentration range of toxic metals ions
362 (2.5 μM to 2 mM) (Fig. 1, and Supplemental Fig. S2-S4). *Mtb* SufB precursor protein (95.98 KDa)
363 follows a canonical intein splicing pathway yielding 40.2 KDa SufB intein and 55.7 KDa ligated

364 exteins (functional SufB protein) as illustrated in Supplemental Fig. S1(62). N-terminal cleavage
365 products (65.26 KDa N-terminal cleavage product, 29.9 KDa N-extein) and C-terminal cleavage
366 products (70.12 KDa C-terminal cleavage product, 25.76 KDa C-extein) are the byproducts of *Mtb*
367 SufB splicing reaction (62).

368 Purified *Mtb* SufB precursor protein was refolded in presence of test metal ions and then resolved
369 through 4~10% gradient SDS PAGE (Fig. 1A). $Cd^{2+}$ at 25 μM, and $Hg^{2+}$ at 500 μM of minimum
370 effective concentration (MEC) displayed significant attenuation of splicing and N-terminal
371 cleavage reactions. There was a noticeable accumulation of SufB precursor protein, along with
372 substantial reduction in the splicing products (ligated exteins and intein). Further, $Cd^{2+}$, and $Hg^{2+}$
373 at their respective MEC values and higher, induced a near-complete inhibition of N-terminal
374 cleavage reaction and the products (N-terminal cleavage product and N-extein) (Fig. 1A).
375 However, $Cr^{3+}$ and $Pb^{2+}$ failed to induce any effect on *Mtb* SufB splicing or cleavage reactions
376 across the test concentration range (Fig. 1A). Resultant protein products were further confirmed
377 via western blot using anti-6X(His) tag antibody (Supplemental Fig. S2). Densitometric analysis
378 revealed a 12.52-fold ($p<0.0001$) reduction in splicing efficiency and an 18.7-fold ($p<0.0001$)
379 reduction in N-terminal cleavage efficiency with 25 μM $Cd^{2+}$ [Fig. 1B (i) and C (i)]. Similarly,
380 treatment with 500 μM $Hg^{2+}$ resulted in an 8-fold ($p < 0.0001$) reduction in splicing and a 7.8-fold
381 ($p < 0.0001$) decrease in N-terminal cleavage efficiency [Fig. 1B (ii) and 1C (ii)]. No significant
382 alterations in SufB splicing or N-terminal cleavage products were obtained in presence of $Cr^{3+}$ or
383 $Pb^{2+}$ (Fig. 1B and 1C). All the test metal ions at a lower concentration range (2.5 μM- 10 μM)
384 failed to exert any significant effect on the SufB splicing reactions (Supplemental Fig. S3 and S4).
385 In order to rule out the possibility of precursor protein degradation by test metal ions, splicing
386 inactive (SI) *Mtb* SufB double mutant (C1A/N359A) was refolded under similar experimental

conditions (25 µM $Cd^{2+}$, 500 µM $Hg^{2+}$, 2 mM $Cr^{3+}$, and 2 mM $Pb^{2+}$). Since $Cr^{3+}$, and $Pb^{2+}$ showed no regulatory effects, highest test concentration range for both were included in the above study. SDS-PAGE and subsequent western blot analysis using anti-6X(His) tag antibodies confirmed the absence of protein degradation products (Supplemental Fig. S2B).

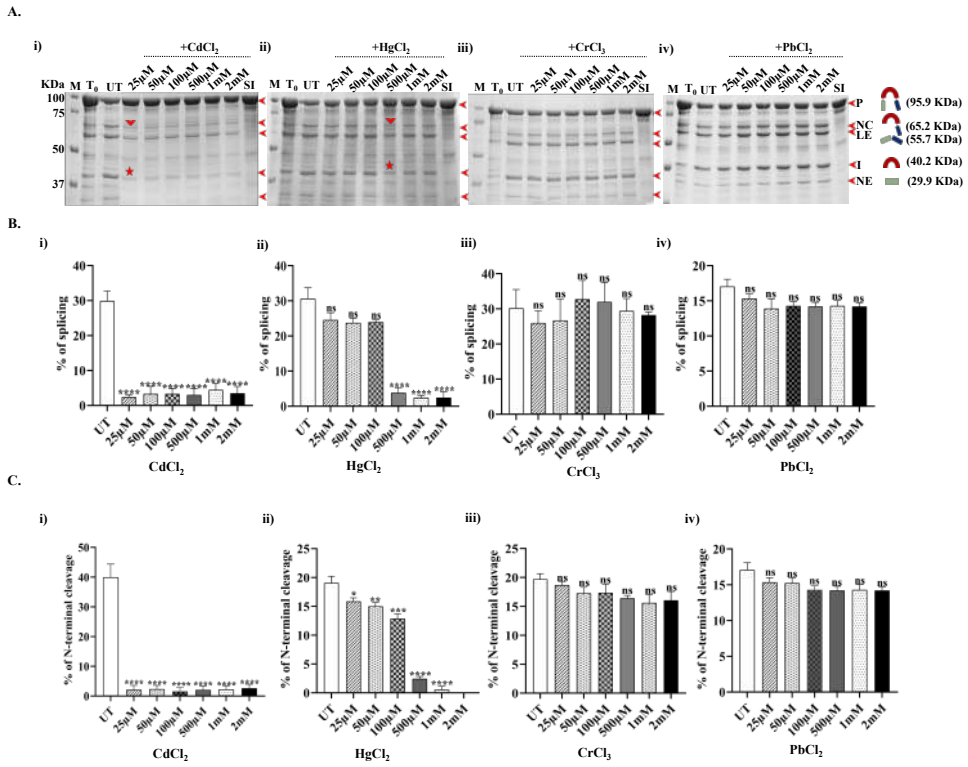


**Fig. 1. Gradient assay to determine the minimum effective concentration (MEC) of toxic metal ions on splicing and N-terminal cleavage reactions of *Mtb* SufB precursor protein. (A)** Following *in vitro* refolding of *Mtb* SufB precursor protein in the presence of (i) $CdCl_2$, (ii) $HgCl_2$, (iii) $CrCl_3$, and (iv) $PbCl_2$ at varied concentrations (25 µM-2 mM), resultant products were resolved through 4~10% gradient SDS-PAGE. Lane 1: Protein ladder; Lane 2 ($T_0$): splicing and N-terminal cleavage reactions at 0 h; Lane 3 (UT): splicing and N-terminal cleavage products of untreated protein sample; Lanes 4-9: splicing and N-terminal cleavage products resulting in the presence of different toxic metal ions at different concentrations (25 µM-2 mM). Lane 10 (SI): splicing inactive SufB double mutant (C1A/N359A) is used as a negative control for splicing. **(B) and (C)**

410 Bar graphs demonstrating splicing and N-terminal cleavage efficiency of *Mtb* SufB precursor
411 protein in the presence and absence of different toxic metal ions. A statistically significant
412 difference in splicing and N-terminal cleavage reaction was observed for B (i) and C (i) $CdCl_2$,
413 starting with 25 µM, and B (ii) and C (ii) $HgCl_2$ at 500 µM concentrations, respectively. For $CrCl_3$
414 [B (iii) and C (iii)], and $PbCl_2$ [B (iv) and C (iv)], no significant difference in splicing and N-
415 terminal cleavage reaction were observed between untreated and metal-treated samples. Graphs
416 were plotted after densitometric analyses using GelQuant.Net biochemical solutions. All the
417 experiments were performed in triplicate, and error bars represent (±1) SEM from 3 independent
418 sets of experiments. The data shown in Fig. 1B, and 1C are extracted from Fig. 1A. M: Prestained
419 protein molecular weight ladder, P: Precursor, NC: N-terminal cleavage product, LE: Ligated
420 extein, I: intein, NE: N-extein.

421

422 Further, a time-dependent splicing assay was performed to examine *Mtb* SufB splicing and
423 cleavage activity over a period of 10 min- 4 hr., elucidating remarkable inhibitory roles of $Cd^{2+}$
424 (25 µM) and $Hg^{2+}$ (500 µM) as early as 10 minutes (Supplemental Fig. S5). Next, to evaluate the
425 possible physical interaction between *Mtb* SufB protein and the metal ions, a series of experiments
426 were conducted, as shown in the upcoming section. For the said interaction study, the MEC for
427 $Cd^{2+}$, $Hg^{2+}$ (25 µM, 500 µM, respectively), which inhibited *Mtb* SufB splicing was selected. Since,
428 $Cr^{3+}$, and $Pb^{2+}$ did not exhibit any such regulatory activity, highest value of the test concentration
429 range (2 mM) was chosen to examine possible interaction with SufB protein.

430 **Protein~ metal interaction study**

431 ***UV-Visible spectroscopic analysis***

432 Biomolecules such as proteins exhibit a strong affinity for metal ions, which can critically
433 influence their structure and function (93). Prior studies have demonstrated that toxic metal ions
434 such as $Cd^{2+}$, $Hg^{2+}$, $Cr^{3+}$, and $Pb^{2+}$ can interact with calcium and zinc-binding sites in proteins,
435 thereby influencing their biological activity (94, 95). UV-visible spectroscopic analysis was
436 conducted to investigate the interaction between the *Mtb* SufB precursor protein and toxic metal

437 ions under treated and untreated conditions. Absorbance spectra for *Mtb* SufB protein were
438 recorded over 200-800 nm range at 25 °C (Supplemental Fig. S6). A characteristic absorbance
439 peak near 280 nm was detected, primarily attributable to aromatic residues such as tryptophan and
440 tyrosine (96, 97). Upon treatment with $Cd^{2+}$, an increase in absorbance intensity was noted,
441 suggesting an alteration in conformation due to metal coordination [Supplemental Fig. S6 (i)].
442 Previous studies have mentioned that enhanced absorbance may result from the interaction
443 between $Cd^{2+}$ and electron-donating groups such as amide, imidazole, and amine (68, 98, 99).
444 Likewise, samples treated with $Hg^{2+}$ also exhibited an increase in absorbance intensity
445 [Supplemental Fig. S6 (ii)]. This enhancement is likely attributed to the strong affinity of $Hg^{2+}$ for
446 nucleophilic functional groups, particularly the sulfhydryl (–SH) groups of cysteine residues (100,
447 101). Although there were sharp increments in absorbance peak following interaction of $Cr^{3+}$and
448 $Pb^{2+}$ with *Mtb* SufB, they failed to exert any effects on SufB splicing reactions as shown earlier
449 (Fig. 1). Moreover, a strong buffer-$Pb^{2+}$ interaction was observed from the results, which may have
450 weakened likely interaction with the protein. Although prior works have shown interaction of $Cr^{3+}$,
451 and $Pb^{2+}$ with thiol, glutathione groups within protein structure including oxygen, nitrogen, and
452 sulfur containing amino acids (7, 102, 103), current work could not detect any effects of these
453 metal ions on *Mtb* SufB splicing activity [Supplemental Fig. S6 (iii and iv)]. To further substantiate
454 such interactions, tryptophan fluorescence spectroscopy was performed, as explained in the
455 forthcoming section.

456 ***Tryptophan Fluorescence spectroscopy reveals metal-induced conformational changes in Mtb***
457 ***SufB***

458 Tryptophan fluorescence spectroscopy is a widely utilized technique for monitoring alterations in
459 protein conformation and assessing local structural dynamics upon interaction with ligands or

460 macromolecules (104). Among the intrinsic fluorophores in proteins, aromatic amino acids—
461 tryptophan (Trp), tyrosine (Tyr), and phenylalanine (Phe)—contribute to fluorescence, with
462 tryptophan exhibiting the highest molar absorptivity (1614 $cm^{-1}/M$) and a characteristic emission
463 peak in the range of 340–350 nm (105). The indole ring of Trp is primarily responsible for this
464 emission and dominates the fluorescence profile over Tyr and Phe. Changes in the
465 microenvironment of tryptophan residues, such as those caused by ligand binding, protein folding,
466 or metal interaction, can lead to measurable shifts in fluorescence intensity and/or emission
467 maxima (104, 106).

468 Altogether, 13 Trp residues are present, spanning the entire sequence of *Mtb* SufB precursor
469 protein, with 5 Trp in N-extein, 5 Trp in Intein, and 3 Trp in the C-extein region (43). Upon
470 treatment with $Cd^{2+}$ (25 μM), an increase in fluorescence intensity was observed [Supplemental
471 Fig. S7 (i)], likely attributable to conformational rearrangements arising from interactions between
472 $Cd^{2+}$ and functional groups such as amide, imidazole, and amine moieties within the protein matrix
473 (68, 98, 99). These interactions may have led to reduced solvent exposure of Trp residues or
474 stabilized a more rigid protein conformation, which enhanced fluorescence emission (68, 107). In
475 contrast, $Hg^{2+}$ (500 μM) treated samples displayed a significant quenching of Trp fluorescence
476 [Supplemental Fig. S7 (ii)]. This effect is consistent with previous studies indicating that mercury
477 ions interact strongly with aromatic systems through cation–π interactions, particularly with the
478 indole ring of tryptophan, thereby reducing fluorescence emission (108). $Cr^{3+}$ (2mM) exposure
479 resulted in a slight increase in fluorescence intensity [Supplemental Fig. S7 (iii)], potentially due
480 to the preferential binding of $Cr^{3+}$ to carboxyl groups, which may induce localized structural
481 stabilization without extensive perturbation of the overall tertiary structure (109, 110). In case of
482 $Pb^{2+}$ (2 mM), a decrease in fluorescence intensity was observed [Supplemental Fig. S7 (iv)]. This

483 observation is supported by previous literature, where $Pb^{2+}$ interacts with hydroxy, amino, and
484 sulfhydryl groups, leading to partial protein unfolding and increased solvent accessibility of Trp
485 residues, thereby promoting fluorescence quenching (111, 112). Although $Cr^{3+}$, $Pb^{2+}$ have
486 displayed possible alteration in protein conformation, they failed to regulate *Mtb* SufB splicing
487 and cleavage reactions, likely due to lack of any effect on protein active site. Next, ICP-OES
488 analysis was conducted to further ascertain potential interaction between test metal ions and
489 protein backbone, as described in the following section.

490 ***ICP-OES detects metal ions bound to SufB precursor and spliced out protein fractions***

491 ICP-OES is a sensitive analytical technique capable of detecting trace metal concentrations by
492 measuring the characteristic emission of photons from the excited atoms and ions as they return to
493 their ground state (113). During *in vitro* protein refolding experiment, specific concentrations of
494 $Cd^{2+}$ (25 µM = 4.583 µg/ml), $Cd^{2+}$ (500 µM = 91.66 µg/ml), $Hg^{+2}$ (500 µM = 135.76 µg/ml), $Cr^{+3}$
495 (2 mM = 361.72 µg/ml), and $Pb^{+2}$ (2 mM = 556.2 µg/ml) were added to the respective reaction
496 mixture. ICP-OES analysis of the metal-bound protein fractions revealed detectable levels of $Cd^{2+}$
497 (2 ppb ~ 0.002 µg/ml), $Hg^{2+}$ (5 ppb, ~0.005 µg/ml), and $Cr^{3+}$ (80 ppb, ~0.08 µg/ml) bound to the
498 unspliced *Mtb* SufB precursor protein (Table 2). These findings indicate a direct and quantifiable
499 physical interaction between the test metal ions and *Mtb* SufB precursor protein, which may
500 underlie the observed inhibition of splicing and N-terminal cleavage reactions. Further, measurable
501 interactions were observed between the test metal ions and various splicing products (ligated extein
502 and intein) (Table 2). $Cd^{2+}$ addition to SufB protein sample at 25 µM concentration yielded
503 negative results, while increasing the concentration to 500 µM led to positive data. At lower
504 concentrations of $Cd^{2+}$ (25 µM), the metal content in the protein fraction was possibly below the
505 instrument's limit of detection (LOD) and limit of quantification (LOQ), resulting in negative

506 readings. Although ICP-OES is capable of detecting metal concentrations at the ppb level, practical
507 detection limits are influenced by matrix complexity and background interference, often resulting
508 in quantification thresholds closer to the ppm range (114–116). Although 80 ppb (0.08 µg/ml) of
509 $Cr^{3+}$ was bound to the unspliced precursor (Table 2), it failed to exert any visible effects on *Mtb*
510 SufB splicing reactions (Fig. 1). No bound form of metal ions were detected in $Pb^{2+}$ treated
511 samples, even at 2 mM concentration (Table 2), consistent with no visible effect on *Mtb* SufB
512 splicing (Fig. 1).

513 **Table 2:** Quantitative elemental detection via ICP-OES analysis: Measurable concentration of
514 metal ions ($Cd^{2+}$, $Hg^{2+}$, $Cr^{3+,}$ and $Pb^{2+}$) were identified bound to *Mtb* SufB precursor and splicing
515 products. P: Precursor, LE: Ligated extein, I: Intein.

516

517

| Metal ions | Treated concentration | Concentration (µg/ml) | ICP-OES values (ppb) | Equivalent Concentration (µg/ml) |
|---|---|---|---|---|
| Cadmium ($Cd^{2+}$) | 25µM | 4.583 | P: -9<br>LE: -5<br>I: -8 | P: -0.009<br>LE: -0.005<br>I: -0.008 |
| Cadmium ($Cd^{2+}$) | 500 µM | 91.66 | P: 2<br>LE: 18<br>I: 1 | P: 0.002<br>LE: 0.018<br>I: 0.001 |
| Mercury ($Hg^{2+}$) | 500 µM | 135.76 | P: 5<br>LE: 3<br>I: 5 | P: 0.005<br>LE: 0.003<br>I: 0.005 |
| Chromium ($Cr^{3+}$) | 2mM | 361.72 | P: 80<br>LE: 83<br>I: 90 | P: 0.08<br>LE: 0.083<br>I: 0.09 |
| Lead ($Pb^{2+}$) | 2mM | 556.2 | P: -17<br>LE: -5<br>I: -73 | P: -0.017<br>LE: -0.005<br>I: -0.073 |

518
519
520
521
522
523
524
525

526 Collectively, the protein refolding assays, along with protein~metal interaction studies, suggested
527 possible interaction of $Cd^{2+}$ and $Hg^{2+}$ with *Mtb* SufB precursor protein, thereby attenuating the
528 splicing and N-terminal cleavage efficacy. These mechanistic insights led to the development of a
529 whole-cell biosensing platform utilizing H37Ra (*Mtb* attenuated strain) as the indicator cells to
530 detect metal ions.

531 Fe-S clusters are essential cofactors for distinct metabolic pathways and cellular processes such as
532 respiration, DNA replication and repair, and persistence under oxidative and nitrosative stress
533 conditions (117–119). SUF complex offers the sole pathway for Fe-S cluster biogenesis in
534 mycobacteria, and its activity relies on the generation of functional SufB protein via protein
535 splicing (60, 61). Besides, there are earlier reports on loss of cellular viability as a result of SufB
536 splicing inhibition within mycobacteria (40, 43, 56). Since, toxic metal ions like of $Cd^{2+}$ and $Hg^{2+}$
537 were shown to inhibit *Mtb* SufB splicing and N-terminal cleavage activity (Fig. 1), an attenuated
538 strain of *Mtb* (H37Ra) was used as the whole-cell viability indicator for these metal ions.

539 **H37Ra- based whole-cell biosensor detects toxic metal ions**

540 Cell-based biosensors are gaining interest as a screening platform for biologically active molecules
541 due to their ability to monitor the cellular functions and interactions with targets in their natural
542 environment (120, 121). Often, they are fabricated as genetically modified biosensors using native
543 receptors or enzymes as molecular recognition elements in living cells (28). Current work explores
544 the use of whole-cell mycobacteria (H37Ra)-based biosensor to detect toxic metal ions like $Cd^{2+}$
545 and $Hg^{2+}$. A 96-well plate assay was developed using Alamar Blue reagent, employing *Mtb*
546 (H37Ra) cells as the sensing component, and *M. sm* cells as the SufB intein-less cellular control
547 (56, 62, 122). *M. sm* carries three intein-bearing proteins: DnaB, which contains two inteins

548 (DnaBi1 and DnaBi2), as well as GyrA and PhoH (49, 64). Although splicing regulation has been
549 shown for DnaBi1 helicase, studies on the DnaBi2, PhoH, GyrA inteins splicing have not been
550 reported yet. DnaBi1 splicing is regulated by zinc and oxidative stressors (49, 64); however, its
551 helicase function can be compensated by other cellular helicases (123–125).

552 Alamar Blue reagent is a non-toxic, resazurin-based solution that functions as an indicator for cell
553 viability (74, 126). The blue-colored non-fluorescent resazurin (7-hydroxy-3H-phenoxazin-3-one
554 10-oxide) gets reduced to resorufin (7-hydroxy-3H-phenoxazin-3-one, pink colored compound)
555 by mitochondrial reductase in metabolically active cells (127). In a comparative study, non-viable
556 H37Ra were visualized in presence of $Cd^{2+}$ and $Hg^{2+}$, whereas persistence of viable *M. sm* cells
557 during the metal-interaction process highlighted the absence of metal sensing SufB precursor
558 protein. Untreated H37Ra cells grown in 7H9 (supplemented with OADC) media, and Alamar
559 Blue reagent alone in 7H9 (supplemented with OADC) media, served as the negative and positive
560 controls for the study respectively.

561 Fig. 2 (i) is a schematic representation of 96-well plate-based biosensor platform containing *Mtb*
562 H37Ra cells (indicator organisms) incubated with varied concentrations of $Cd^{2+}$ (2.5 μM -2 mM)
563 and $Hg^{2+}$ (25 μM -2 mM). The test concentration range for the metal ions were chosen based on
564 the positive results obtained during *in vitro* splicing analyses (Fig. 1, Supplemental Fig. S2-S4).
565 For a baseline correction, H37Ra cells were grown in the absence of toxic metal ions (negative
566 control). SufB intein-less, *M. sm* cells were used as additional experimental control. Unlike *Mtb*
567 H37Ra cells, the growth and viability of the *M. sm* cells are independent of SufB intein splicing,
568 and any loss of cell viability indicates metal toxicity. Fig. 2 (ii) shows that the indicator cells
569 (H37Ra) incubated in the presence of lower concentration of $Cd^{2+}$ (2.5-10 μM) did not lose cell
570 viability. All the cells were metabolically active and converted resazurin (blue) to resorufin (pink),

571 since $Cd^{2+}$ at these concentration (2.5-10 μM) didn't affect SufB splicing activity, generating
572 active SufB protein [Supplemental Fig. S3 (i)]. H37Ra cells incubated in presence of 25 and 50
573 μM of $Cd^{2+}$, displayed purple color indicating a partial loss of cell viability, underscoring 25 μM
574 as the minimum inhibitory concentration (MIC). Cells incubated with $Cd^{2+}$ at a concentration range
575 of 100 μM- 2 mM, retained blue color, indicating complete loss of cell viability. These results
576 correlated to inhibition of splicing and N-terminal activity of *Mtb* SufB in presence of $Cd^{2+}$ over a
577 concentration of 25 μM - 2 mM (Fig. 1).

578 Next, cells incubated in the presence of 25 μM and 50 μM of $Hg^{2+}$ resulted in healthy viable (pink)
579 cell population, whereas cells in the presence of 100 μM $Hg^{2+}$ exhibited purple color, highlighting
580 partial loss of cell viability at MIC value. Over rest of the concentration range for $Hg^{2+}$ (500 μM-
581 2 mM), non-viable (blue) cells were noticed. These results were supported by SufB splicing
582 attenuation by $Hg^{2+}$ (500 μM-2 mM), while a lower concentration (2.5 μM-10 μM) $Hg^{2+}$ failed to
583 exert any such effects (Fig. 1, Supplemental Fig. S4). Although 100 μM of $Hg^{2+}$ didn't influence
584 SufB splicing, the N-terminal cleavage reaction was reduced significantly, marking this as the MIC
585 value with partial loss of cell viability. Summarizing, persistence of blue color in the presence of
586 $Cd^{2+}$ (100 μM until 2 mM), and $Hg^{2+}$ (500 μM until 2 mM) may be correlated to complete loss of
587 H37Ra viability due to inhibition of *Mtb* SufB splicing and N-terminal cleavage reactions (Fig. 1).
588 These results suggest the potential use of mycobacterial (H37Ra) cells as the biological indicator
589 for a qualitative toxic metal detection.

590

591

592

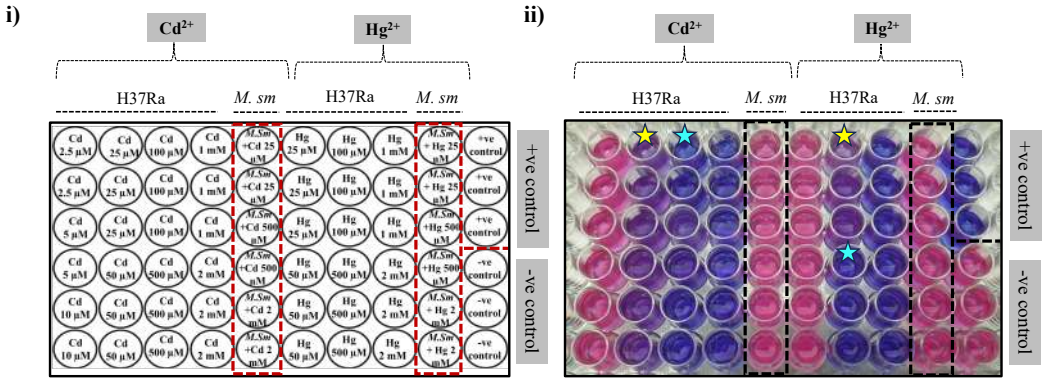


**Fig. 2. 96-well plate-based biosensor assay demonstrating whole cell mycobacteria (*Mtb* H37Ra strain) as the biological indicator for toxic metal ions ($Cd^{2+}$ and $Hg^{2+}$)** (i) Schematic representation of 96 well plate-based Biosensor platform. (ii) H37Ra cells ($10^8$ CFU/ml) were seeded in the presence of varied concentration ranges of $CdCl_2$ (2.5 µM- 2 mM) and $HgCl_2$ (25 µM- 2 mM), respectively. Cells incubated in the presence of $CdCl_2$ (2.5 µM- 10 µM) and $HgCl_2$ (25 µM- 50 µM) were pink in color indicating healthy viable cells resisting the splicing inhibitory effect of the metal ions. In contrast, cells exposed to $CdCl_2$ (25 µM and 50 µM) and 100 µM of $HgCl_2$ displayed purple color suggesting partial loss of cell viability. Cells incubated with 100 µM- 2 mM of $CdCl_2$ and 100 µM- 2 mM of $HgCl_2$ remained blue, suggesting complete loss of viable cell population. For a baseline correction, test organisms were allowed to grow in the absence of toxic metal ions and denoted as live cell control (negative control). SufB intein-less organism *Mycobacterium smegmatis (M. sm)* was used as additional experimental control and treated under similar conditions. *M. sm* cells exhibited pink color across a varied range of toxic metal ions, suggesting their cell viability as an intein-independent phenomenon. The experiments were performed in triplicates to confirm the reproducibility of data. Cyan stars- complete loss of viability (blue) & Yellow stars- partial loss of viability (purple).

Next, a quantitative analysis for the toxic metal ions was performed by measuring the absorbance of Alamar Blue reagent at 570 nm with 600 nm as a reference wavelength (74). Metal samples of known concentrations were prepared and loaded on to the 96-well plate and treated with Alamar Blue reagent under optimised experimental conditions [Fig. 3 (i)-(iv)]. A standard graph was generated by plotting the absorbance values of Alamar reagent vs the known concentrations of test

metal ions ($Cd^{2+}$ and $Hg^{2+}$) [Fig. 3 (v) and (vi)]. Subsequently, a linear regression analysis was performed to determine the equation of the line, expressed as y = mx + c. To further validate the standard plot, unknown samples with varying concentrations of $Cd^{2+}$ ions and $Hg^{2+}$ ions were prepared (Experimental Procedure). Absorbance values of the unknown samples were extrapolated onto standard graph to determine the concentrations of $Cd^{2+}$ and $Hg^{2+}$ (Fig. 3 (v), (vi) and Table S1). Unknown samples with concentration higher than the standard range may be adjusted via dilution, or the standard calibration plot may be extended to higher concentration ranges (128). However, sample concentration at a value lower than the standard range may not be determined accurately possibly due to no effect on intein splicing and hence no loss of cell viability.

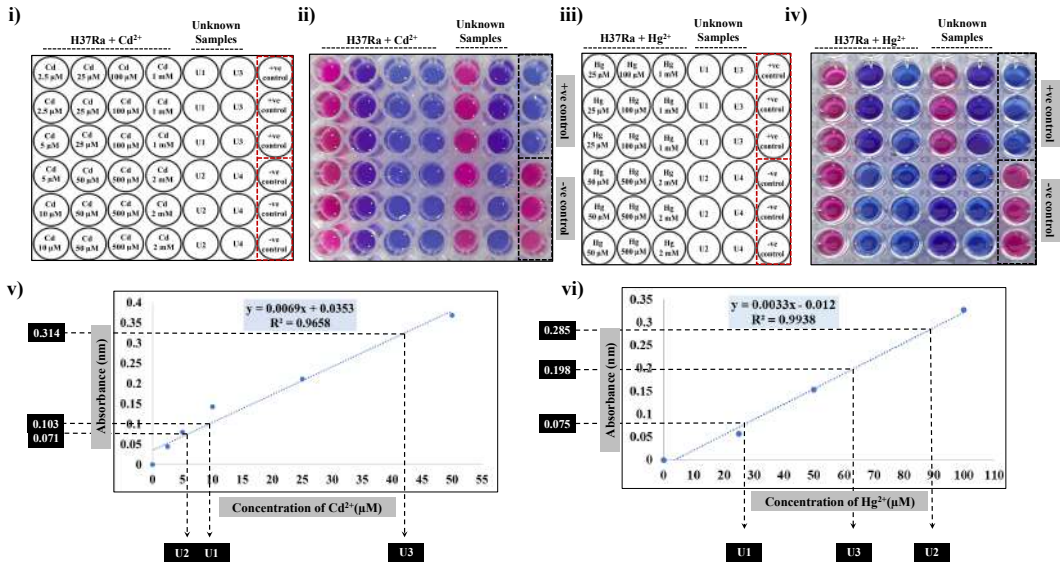


**Fig. 3. Standard curve for quantitative determination of $Cd^{2+}$ and $Hg^{2+}$ concentrations.** (i), and (iii) Schematic representations of H37Ra-based Biosensor platform to detect $CdCl_2$ and $HgCl_2$. (ii), and (iv) *Mtb* H37Ra cells were grown in presence of varied concentration of $CdCl_2$ and $HgCl_2$. To establish a baseline, test organisms were allowed to grow in absence of toxic metal ions (live cell or negative control). (v), and (vi) The absorbance values of the Alamar Reagent solutions were plotted along the y-axis and the known concentrations of $Cd^{2+}$ and $Hg^{2+}$ were plotted along the x-axis. A linear regression analysis was conducted to obtain the equation for the line, and used to determine the concentration of unknown samples. The experiments were performed in triplicates

645 to confirm the reproducibility of data.

646

647 Next, to elucidate the specificity of the designed biosensor platform, $Cd^{2+}$- and $Hg^{2+}$- specific
648 metal chelators, Edetate Calcium Disodium (ECD), and meso-2,3-Dimercaptosuccinic acid
649 (DMSA) were incubated alongside the test samples (129–134). Fig. 4 (i) is a schematic
650 representation of the biosensor platform, where indicator mycobacterial cells were exposed to $Cd^{2+}$
651 and $Hg^{2+}$, in presence of $Cd^{2+}$-specific chelator, ECD. Fig. 4 (ii) demonstrates that ECD effectively
652 resisted $Cd^{2+}$- induced loss of viability, resulting in healthy cells that transformed resazurin (blue)
653 to resorufin (pink). Conversely, ECD failed to restore viability of $Hg^{2+}$ treated cells, where
654 inhibition of SufB splicing, rendered non-viable (blue) cells. Next, mycobacterial cells were
655 subjected to varying concentrations of $Cd^{2+}$ and $Hg^{2+}$, supplemented with metal chelator DMSA
656 ($Hg^{2+}$ specific) [Fig. 4 (iii) and (iv)]. $Hg^{2+}$ treated H37Ra cells remained viable in presence of
657 DMSA, while $Cd^{2+}$ continued its inhibitory effect on SufB splicing inducing non-viable (blue)
658 cells. These observations affirmed the specificity of the designed biosensor platform to detect
659 toxic metal ions $Cd^{2+}$ and $Hg^{2+}$.

660

661

662

663

664

665

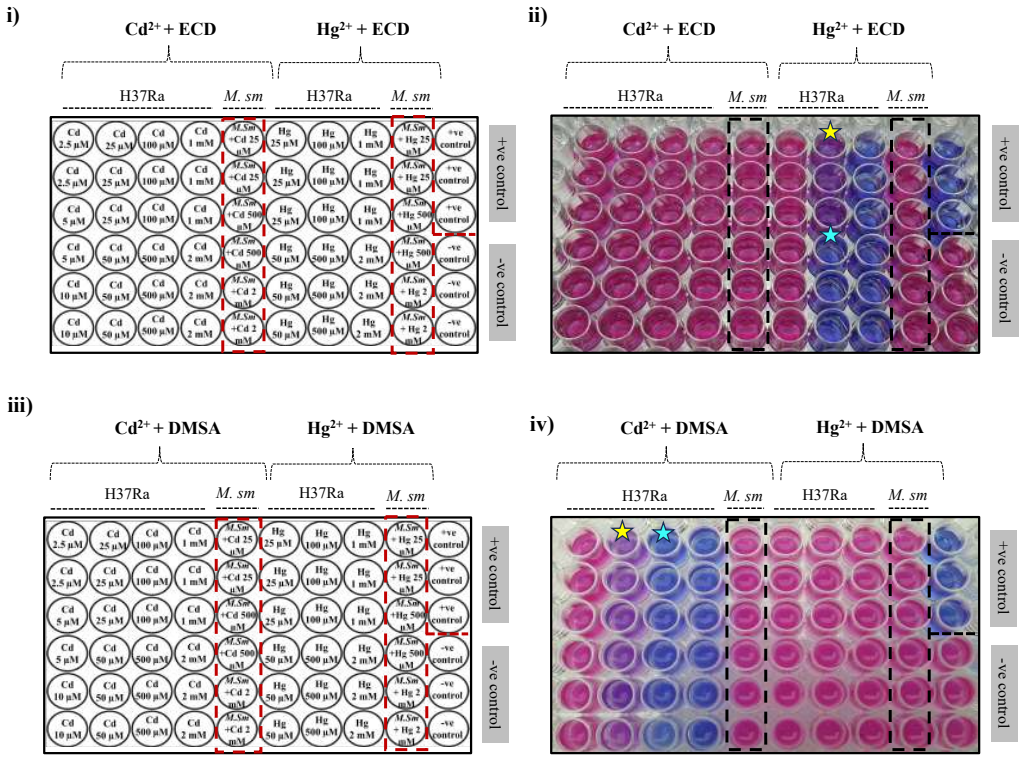


**Fig. 4. Determination of the specificity of *Mtb* H37Ra-based biosensor platform using metal chelators.** (i) Schematic representation of the biosensor platform including $Cd^{2+}$ specific metal chelator (ECD) (ii) *Mtb* H37Ra cells ($10^8$ CFU/ml) were allowed to grow in presence of varied concentration range of $CdCl_2$ and $HgCl_2$, along with ECD (1:1 ratio). ECD reversed the inhibitory effect of $Cd^{2+}$ inducing viable (pink) cells, whereas the effect of $Hg^{2+}$ persisted (iii) Schematic representation of the biosensor platform including $Hg^{2+}$ specific metal chelator (DMSA). (iv) *Mtb* H37Ra cells ($10^8$ CFU/ml) were allowed to grow in the presence of varied concentration ranges of $CdCl_2$ and $HgCl_2$, including DMSA in the ratio 1:1. DMSA blocked the inhibitory effect of $Hg^2$, rendering pink viable cells, whereas the effect of $Cd^{2+}$ persisted. For a baseline correction, H37Ra cells were grown in the absence of toxic metal ions as the live cell control. SufB intein-less organism *Mycobacterium smegmatis (M. sm)* was used as additional experimental control and treated under similar conditions. *M. sm* cells exhibited pink color across a varied range of toxic metal ions, suggesting their cell viability as an intein-independent phenomenon. The experiments were performed in triplicates to confirm the reproducibility of data. Cyan stars- complete loss of viability (blue) & Yellow stars- partial loss of viable cells (purple). ECD: Edetate Calcium disodium, DMSA: Meso-2,3-Dimercaptosuccinic acid.

692 Next for a multiplex metal screening process, the efficacy of the platform was assessed in presence
693 of known splicing inhibitors $Zn^{2+}$ (100 µM-2 mM), $Cu^{2+}$ (100 µM-2 mM), $Pt^{4+}$ (20 µM-1 mM)
694 along with $Cd^{2+}$ (10 µM-2 mM) and $Hg^{2+}$ (25 µM-2 mM) (Fig. 5) (43). Baseline correction was
695 achieved by growing H37Ra cells in the absence of toxic metal ions (negative control), while SufB
696 intein-less *M. sm* cells served as additional experimental control. Cells treated with 100 µM $ZnCl_2$
697 and $CuCl_2$, 20 µM $PtCl_4$, 10 µM $CdCl_2$, and 25 µM $HgCl_2$, turned pink in color, indicating intact
698 viability. At intermediate concentrations, 600 µM of $ZnCl_2$ and $CuCl_2$, 40 µM $PtCl_4$, 25 µM $CdCl_2$,
699 and 100 µM $HgCl_2$, a transition from blue to purple color was observed, suggesting partial loss of
700 cell viability. Complete loss of viability was noted at higher concentration range, for $ZnCl_2$ and
701 $CuCl_2$ (800 µM- 2 mM), $PtCl_4$ (80 µM- 1 mM), $CdCl_2$ (100 µM- 2 mM), and $HgCl_2$ (500 µM- 2
702 mM) (Fig. 5 ii). Dead non-viable cells induced by $Zn^{2+}$, $Cu^{2+}$, and $Pt^{4+}$ may be correlated to
703 inhibition of *Mtb* SufB splicing and N-terminal cleavage reactions as published earlier (43). In
704 contrast, SufB intein-less organism (*M. sm*) remained viable (pink) under similar experimental
705 conditions, suggesting cell viability as a splicing independent phenomenon. These observations
706 may also be used to rule out metal toxicity on cell viability over the test concentration range.

707

708

709

710

711

712

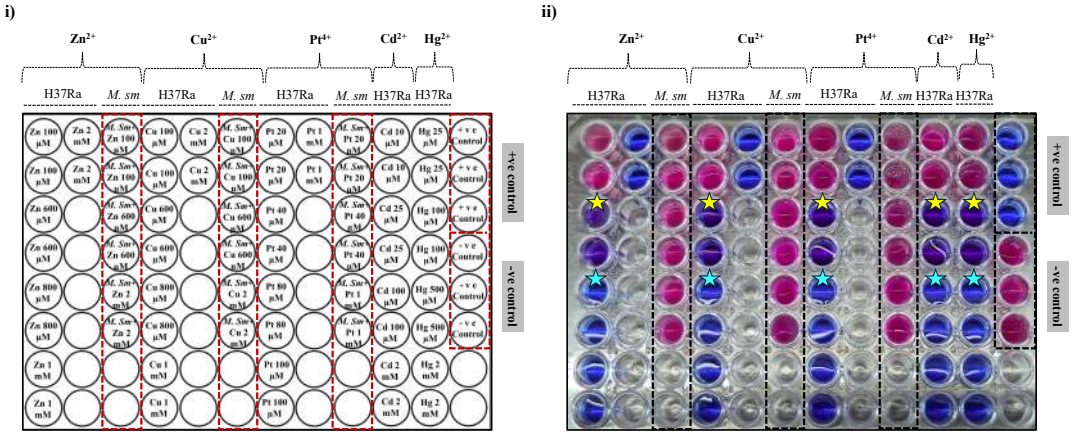


**Fig. 5. Evaluation of *Mtb* H37Ra-based biosensor platform for high-throughput and multiplex detection of trace metal elements and toxic metal ions ($Zn^{2+}$, $Cu^{2+}$, $Pt^{4+}$, $Cd^{2+}$, and $Hg^{2+}$).** (i) Schematic representation of the multiplexing biosensor platform. (ii) H37Ra cells ($10^8$ CFU/ml) were allowed to grow in the presence of $ZnCl_2$ (100 µM- 2 mM), $CuCl_2$ (100 µM- 2 mM), $PtCl_4$ (20 µM- 1 mM), $CdCl_2$ (10 µM- 2 mM) and $HgCl_2$ (25 µM- 2 mM), respectively. Cells incubated with 100 µM of $ZnCl_2$ and $CuCl_2$, 20 µM of $PtCl_4$ , 10 µM of $CdCl_2$ and 25 µM of $HgCl_2$ were pink in color indicating healthy viable cells. In contrast, cells exposed to 600 µM of $ZnCl_2$ and $CuCl_2$, 40 µM of $PtCl_4$ , 25 µM of $CdCl_2$ and 100 µM of $HgCl_2$ turned purple in color suggesting partial loss of cell viability, whereas cells exposed to 600 µM- 2 mM of $ZnCl_2$ and $CuCl_2$, 80 µM- 1 mM of $PtCl_4$ , 100 µM- 2 mM of $CdCl_2$ and 500 µM- 2 mM of $HgCl_2$ remained blue in color suggesting complete loss of viable cell population. For a baseline correction, H37Ra cells were grown in the absence of toxic metal ions as the live cell control (negative control). SufB intein-less organism *Mycobacterium smegmatis (M. sm)* was used as additional experimental control and treated under similar conditions. *M. sm* cells exhibited pink color across a varied range of toxic metal ions, suggesting their cell viability as an intein-independent phenomenon. The experiments were performed in triplicates to confirm the reproducibility of data. Cyan stars- complete loss of viability (blue) & Yellow stars- partial loss of viability (purple).

The multiplexing ability of the biosensor platform was further examined by employing metal-specific chelators along with the metal-treated samples. The $Cd^{2+}$-specific chelator ECD and $Hg^{2+}$-specific chelator DMSA were tested alongside the broad-spectrum metal chelator EDTA. Fig. 6 (i) is a schematic representation of the biosensor platform, where indicator mycobacterial cells were incubated with $Cd^{2+}$-specific chelator, ECD. Fig. 6 (ii) demonstrates that co-incubation with

742 ECD effectively reversed $Cd^{2+}$- induced loss of viability, restoring pink color. This effect was not
743 observed in cells exposed to other metal ions, where ECD could not block metal induced inhibition.
744 Similarly, DMSA reversed the toxic effects of $Hg^{2+}$ [Fig. 6 (iii) and (iv)], while other metal ions
745 continued to attenuate cell viability. Notably, Since EDTA is a broad-spectrum metal chelator, it
746 restored viability across all metal-treated samples [Fig. 6 (v) and (vi)]. Collectively, these findings
747 validate the high-throughput and multiplexing capability of the developed biosensor platform,
748 underscoring its potential for simultaneous detection of multiple toxic metal ions with high
749 specificity and sensitivity.

750

751

752

753

754

755

756

757

758

759

760

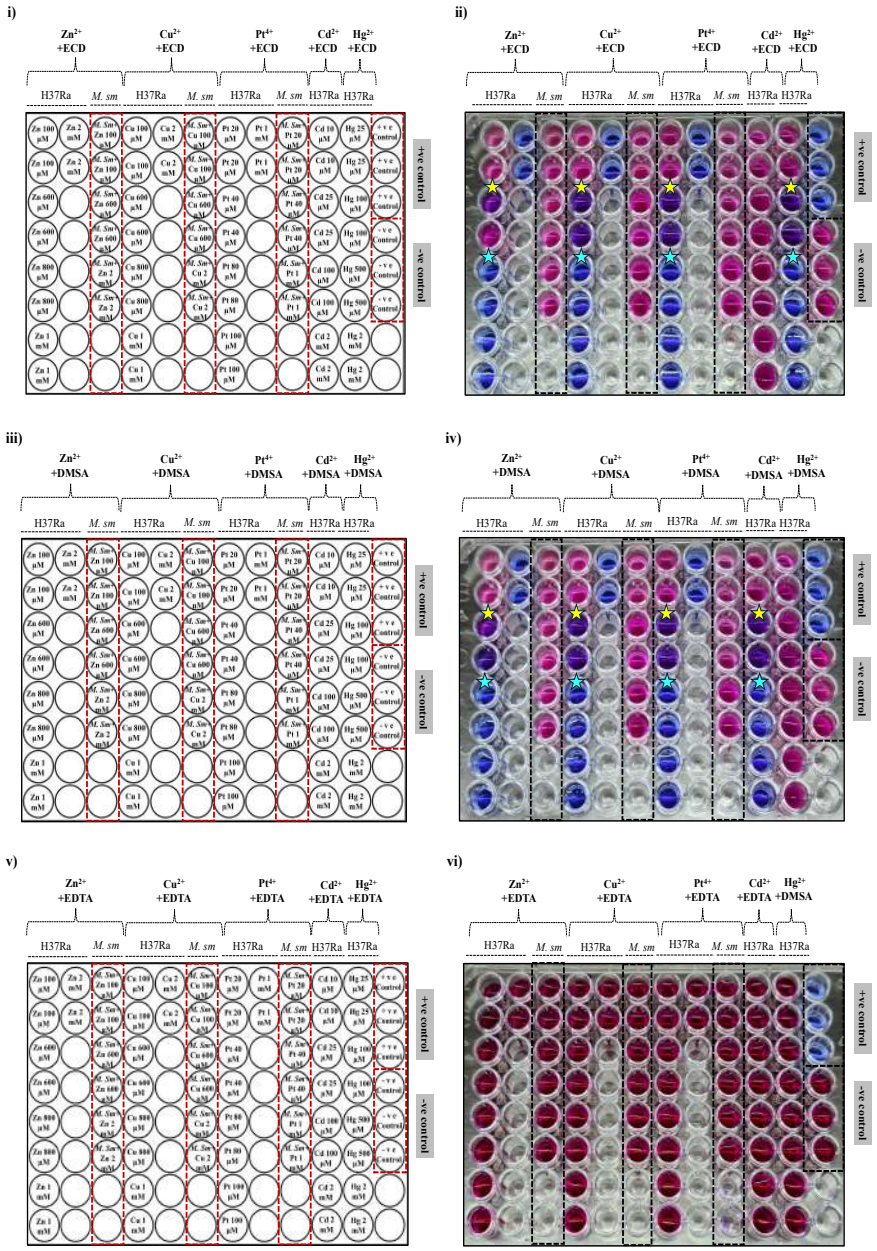


**Fig. 6. Determination of specificity of the *Mtb* H37Ra-based multiplexing biosensor platform.** (i) Schematic representation of the multiplexing biosensor platform along with $Cd^{2+}$ specific metal chelator (ECD) (ii) *Mtb* H37Ra cells ($10^8$ CFU/ml) were incubated with different concentration of $ZnCl_2$ ,$CuCl_2$, $PtCl_4$ , $CdCl_2$ and $HgCl_2$, along with ECD (1:1 ratio). ECD reversed the inhibitory effect of $Cd^{2+}$ rendering viable pink cells, whereas the effects of other metal ions persisted (iii) Schematic representation of the multiplexing biosensor platform along with $Hg^{2+}$ specific metal chelator (DMSA). (iv) *Mtb* H37Ra cells ($10^8$ CFU/ml) were incubated with different concentration

782 of $ZnCl_2$ ,$CuCl_2$, $PtCl_4$ , $CdCl_2$ and $HgCl_2$, along with DMSA in the ratio 1:1. DMSA inhibited the
783 effect of $Hg^{2+}$ inducing viable pink cells, whereas the effect of other metal ions persisted. (v)
784 Schematic representation of plate-based biosensor platform in presence of common metal chelator
785 EDTA. (vi) *Mtb* H37Ra cells ($10^8$ CFU/ml) were allowed to grow in presence of $ZnCl_2$ ,$CuCl_2$,
786 $PtCl_4$ , $CdCl_2$ and $HgCl_2$ along with EDTA in the ratio 1:1. The inhibitory effects of test metal ions
787 on mycobacterial cells were reversed by EDTA. For a baseline correction, H37Ra cells were grown
788 in the absence of toxic metal ions, as the live cell control. SufB intein-less organism
789 *Mycobacterium smegmatis (M. sm)* was used as additional experimental control and treated under
790 similar conditions. *M. sm* cells exhibited pink color across a varied range of toxic metal ions,
791 suggesting their cell viability as an intein-independent phenomenon. The experiments were
792 performed in triplicates to confirm the reproducibility of data. Cyan stars- complete loss of
793 viability (blue) & Yellow stars- partial loss of viable cells (purple). ECD: Edetate Calcium
794 disodium, DMSA: Meso-2,3-Dimercaptosuccinic acid, EDTA: Ethylenediaminetetraacetic Acid.

795

796 In toto, the designed biosensor has demonstrated the potential of whole-cell *Mtb* H37Ra as an
797 indicator to detect toxic metal ions as well as TMEs in test samples. The specificity of the designed
798 metal-sensor was shown by the reversal of the inhibitory effects in the presence of $Cd^{2+}$- and $Hg^{2+}$-
799 specific metal chelators, ECD and DMSA, respectively. Detection of metal ions at a concentration
800 of 25 μM ($Cd^{2+}$) highlights the sensitivity of the biosensor platform, although it requires further
801 optimization to cover the lower concentration range of various metal ions. We propose the use of
802 whole-cell microorganisms carrying metal-sensing intein-bearing proteins as an indicator for the
803 presence of toxic metal ions in environmental samples. This is a user-friendly method that can be
804 performed in a 96-well microtiter plate, which would provide a color change between blue and
805 pink while sensing metal ions. Since the activity of metal-sensing intein-carrying protein
806 sequences are unique for the indicator (whole-cell) organisms, in the unlikely event of
807 contamination in a biological facility, it should not raise concern about the validity of the results.

808

809

810 **Conclusion**

811 Heavy metal ions are persistent environmental contaminants that pose significant risks to both
812 ecological systems and human health. With the rising burden of metal pollution across diverse
813 environmental and biological matrices, there is a pressing need for sensitive, specific, and user-
814 friendly biosensing technology. Intein-mediated biosensors are emerging as promising tools in this
815 context, particularly due to their unique splicing mechanism that operates efficiently under
816 physiological conditions, eliminating the need for external cofactors or energy sources (34, 135).
817 In this study, an innovative biosensor platform was developed, employing native H37Ra cells
818 where intein splicing inhibition is a readout mechanism for the detection of toxic heavy metal ions
819 (e.g., $Cd^{2+}$ and $Hg^{2+}$) and other trace metal elements (Fig. 7). The resulting alteration in
820 mycobacterial viability is captured through a rapid and quantifiable resazurin-based colorimetric
821 assay that reports color change between blue-purple-pink. Importantly, the platform is adaptable
822 for multiplex detection of metal ions, including $Zn^{2+}$, $Pt^{4+}$, $Cu^{2+}$, $Cd^{2+}$, and $Hg^{2+}$, thereby offering
823 a high-throughput solution for complex sample screening (Fig. 5 and 6). Further, this can be
824 extended to sense metal ions by other whole-cell microorganisms, harbouring unique metal-
825 sensing intein-containing proteins, hence offering a qualitative as well as quantitative detection
826 method.

827 SufB is a critical component of SUF system, the exclusive pathway for Fe-S cluster assembly in
828 mycobacteria. Previous studies have also highlighted the pivotal role of *Mtb* SufB protein in Fe-
829 S cluster biogenesis, and mycobacterial survival (61, 136). Since the functionality of SUF protein
830 complex is dependent on generation of active SufB protein via splicing, splicing inhibition presents
831 a promising approach for antimicrobial intervention by targeting mycobacterial viability. Several
832 studies have shown that divalent cations ($Zn^{2+}$and $Cu^{2+}$), ROS, RNS, chlorine derivatives, small

833 molecules (cisplatin and diethanolamine) and zinc oxide nanoparticles can act as potent splicing
834 inhibitors. These agents have influenced mycobacterial survival, further validating the relevance
835 of targeting intein splicing for antimycobacterial drug development (40, 43, 51, 56, 58, 64, 66,
836 137–139). Earlier work from our group has demonstrated that metal ions such as $Cu^{2+}$, $Zn^{2+}$, and
837 $Pt^{4+}$ inhibit SufB splicing, establishing a correlation between metal-induced stress and altered
838 intein splicing activity in *Mtb* (43). Building on these findings, the current work explores
839 regulatory roles of toxic metal ions on *Mtb* SufB splicing and cleavage activity. Alamar Blue assay
840 was employed to examine the influence of TMEs and toxic metal ions on the viability of *Mtb* cells.
841 The outcome of this research will advance the real time application of H37Ra/*Mtb* based whole-
842 cell biosensor to detect wide range of metal ions. The platform described herein is robust, enabling
843 multiplex screening of metal ions while maintaining specificity and sensitivity. Importantly,
844 cellular viability loss in response to metal exposure is linked to an observable color shift between
845 blue and pink, providing a quantifiable readout for metal ion detection in test samples.

846 In this study, splicing inhibition was evaluated both *in vitro*, using purified SufB protein and *in*
847 *vivo* within H37Ra cells in a whole-cell biosensor platform, where the observed effects on
848 mycobacterial viability were correlated to SufB splicing inhibition. Given that H37Ra is a slow-
849 growing strain with a mean generation time of approximately 44 hours, the experimental window
850 was established at four days to encompass at least two full generations, permitting effective
851 assessment of metal-induced viability changes (140–142). Notably, the logarithmic growth phase
852 of mycobacteria extends from four to twenty days, ensuring that the platform remains adaptable to
853 varied experimental requirements. To further strengthen our hypothesis, SufB intein less organism,
854 *M. sm* control was included; viability of *M. sm* persisted throughout the experimental period,
855 suggesting that the tested metal ions do not elicit growth inhibitory or toxic effects in the absence

856 of SufB intein. *Mtb* contains three intein containing proteins; SufB, RecA and DnaB. While SufB
857 is essential for Fe-S cluster assembly, RecA and DnaB play pivotal roles during DNA replication;
858 taken together these proteins are critical for mycobacterial survival (143–145). Although current
859 study explains loss of mycobacterial cell viability as a result of inhibition of *Mtb* SufB splicing,
860 the possibility of RecA and DnaB splicing inhibition by the test metal ions cannot be ruled
861 completely. Currently, there are no literatures to show inhibitory effect of metal ions other than
862 $Zn^{2+}$ on *Mtb* DnaB splicing (49). Moreover there are alternative helicases present in mycobacteria
863 to take over the function of DnaB (123–125). Several studies have reported regulatory roles of
864 $Zn^{2+}$, $Cd^{2+}$, $Co^{2+}$, $Ni^{2+}$, $Cu^{+}$/$Cu^{2+}$, CisPt ions on *Mtb* RecA intein splicing (45, 47, 58, 137).
865 However, current study has not evaluated the RecA intein inhibition in mycobacteria. Hence, this
866 approach offers a multiplexing biosensor unit which can accommodate cell viability detection via
867 splicing inhibition in many organisms carrying different metal-sensitive intein containing proteins
868 simultaneously.

869 The use of non-genetically modified *Mtb* H37Ra cells ensures biosecurity compliance while
870 providing a biologically relevant sensing chassis. These mycobacterial cells are not only easy to
871 cultivate and maintain but also exhibit remarkable long-term viability, supporting extended shelf-
872 life and storage without specialized conditions. The platform also demonstrates good sensitivity in
873 detecting metal ions over a broad dynamic range, and substrate specificity, making it suitable for
874 metal ion screening in standard laboratory setups.

875 However, some limitations persist such as complex environmental or biological samples
876 containing mixtures of multiple metal ions may result in signal overlap or cross-reactivity with
877 variable binding affinities. Furthermore, while microbial whole-cell biosensors offer an excellent
878 alternative for initial screening and field deployment, advanced physicochemical instruments

remain crucial when trace-level quantification is required, where intein activity may not be efficiently regulated.

In summary, our findings highlight the potential of whole cell intein-based biosensors as user-friendly, and cost-effective tools for the detection of toxic metal and trace metal ions. Future work should aim to refine their activity, enhancing environmental robustness, and advancing the platform from lab-scale to deployable technologies. This can be accelerated through collaborative efforts across academic, industrial, and governmental sectors.

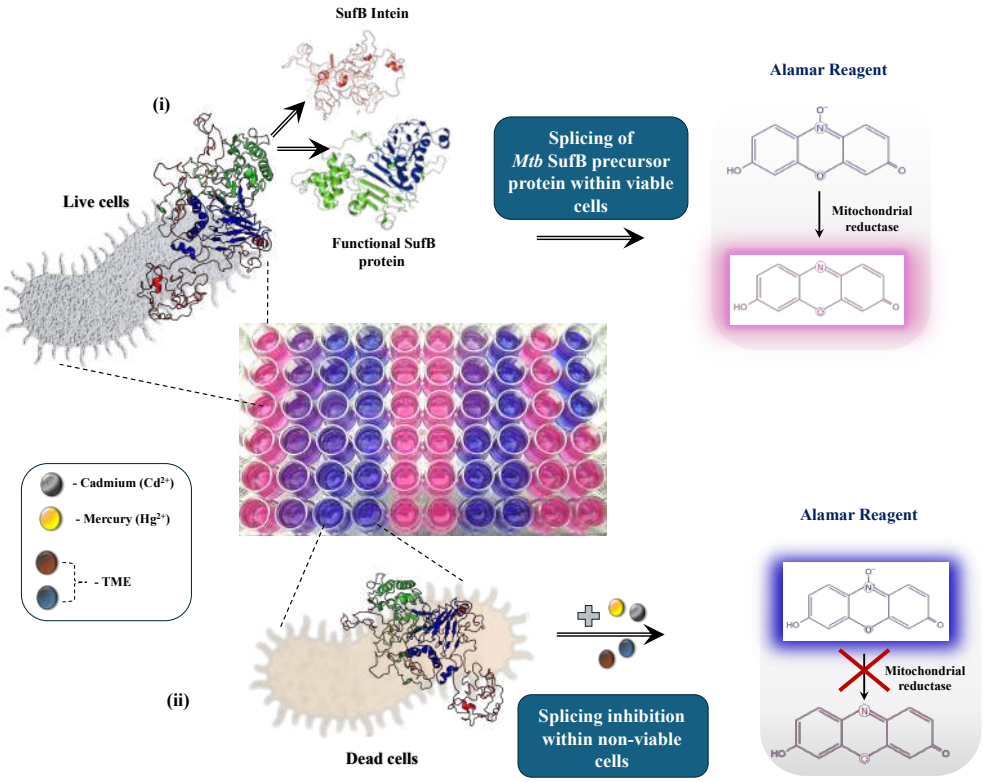


**Fig. 7. Schematic representation explaining the principle of *Mtb* H37Ra-based multiplexing biosensor platform.** Whole-cell mycobacteria (H37Ra) were used as biological indicator for the detection of toxic metal ions ($Cd^{2+}$ and $Hg^{2+}$) and other trace metal elements (TME). (i) Intein

splicing under normal physiological conditions generates functional SufB protein, while viable mycobacterial cells convert resazurin (blue) to resorufin (pink). (ii) In the presence of toxic metal ions $Cd^{2+}$ and $Hg^{2+}$ and TME, SufB intein splicing is inhibited resulting in non-viable mycobacterial cells, thus there is no conversion of resazurin (blue) to resorufin (pink).

## Data availability

The data underlying the present article are available in the article and in its online Supplementary materials. Additional data will be made available on request if needed.

## Supplemental Data

This article contains supplemental data.

## Acknowledgment

The plasmids used in this study are borrowed from Prof. Marlene Belfort's Lab, SUNY, Albany, NY, USA. Our sincere gratitude to the Central Instrumentation Facility (CIF) at OUAT (Odisha University of Agriculture & Technology), Bhubaneswar, and Dr. S.K. Dash for his help in conducting the ICP-OES analysis at OUAT, Bhubaneswar.

## Author Contributions

**AM:** Writing – Original Draft, Writing - Review & Editing, Methodology, Investigation, Formal analysis, Data curation, Visualization, Validation, Software, Resources, Funding acquisition; **AN:** Conceptualization, Methodology, Investigation, Formal analysis, Data curation; Writing - Review & Editing, ; **SN:** Conceptualization, Writing - Original Draft, Writing - Review & Editing, Project administration, Supervision, Methodology, Investigation, Resources, Funding acquisition.

**Funding and Additional Information**

Ms. Ashwaria Mehra is supported by INSPIRE fellowship (DST/INSPIRE/03/2021/002800/IF 190921); INSPIRE Division, DST, Government of India. This work was also supported by the UGC-DAE consortium for scientific research (UGC-DAE-CSR-KC/CRS/15/IOP/08/0562), Kolkata, India.

**Conflict of Interest**

The authors declare that they have no known competing financial interests or personal relationships that could have appeared to influence the work reported in this paper.

943

944 **References**


945 1. Velusamy, K., Periyasamy, S., Kumar, P. S., Rangasamy, G., Nisha Pauline, J. M.,
946 Ramaraju, P., Mohanasundaram, S., and Nguyen Vo, D. V. (2022) Biosensor for heavy
947 metals detection in wastewater: A review. *Food and Chemical Toxicology* 168, 113307

948 2. Duffus, J. H. (2002) *"heavy metals" - A meaningless term? (IUPAC technical report)*
949 (Walter de Gruyter GmbH)

950 3. Turdean, G. L., and Ozkan, S. A. (2011) Design and Development of Biosensors for the
951 Detection of Heavy Metal Toxicity. *International Journal of Electrochemistry* 2011,
952 343125

953 4. Singh, R., Gautam, N., Mishra, A., and Gupta, R. (2011) Heavy metals and living
954 systems: An overview. *Indian J Pharmacol* 43, 246–253

955 5. Angon, P. B., Islam, M. S., KC, S., Das, A., Anjum, N., Poudel, A., and Suchi, S. A.
956 (2024) Sources, effects and present perspectives of heavy metals contamination: Soil,
957 plants and human food chain. *Heliyon* 10, e28357

958 6. Alengebawy, A., Abdelkhalek, S. T., Qureshi, S. R., and Wang, M. Q. (2021) Heavy
959 Metals and Pesticides Toxicity in Agricultural Soil and Plants: Ecological Risks and
960 Human Health Implications. *Toxics* 9, 42

961 7. Jaishankar, M., Tseten, T., Anbalagan, N., Mathew, B. B., and Beeregowda, K. N. (2014)
962 Toxicity, mechanism and health effects of some heavy metals. *Interdiscip Toxicol* 7, 60–
963 72

964 8. Hassani, S., Rezaei Akmal, M., Salek Maghsoudi, A., Rahmani, S., Vakhshiteh, F.,
965 Norouzi, P., Ganjali, M. R., and Abdollahi, M. (2020) High-Performance Voltammetric
966 Aptasensing Platform for Ultrasensitive Detection of Bisphenol A as an Environmental
967 Pollutant. *Front Bioeng Biotechnol* 8, 574846

968 9. Odobašić, A., Šestan, I., Begić, S., Odobašić, A., Šestan, I., and Begić, S. (2019)
969 *Biosensors for Determination of Heavy Metals in Waters* (IntechOpen)

970 10. Ramnani, P., Saucedo, N. M., and Mulchandani, A. (2016) Carbon nanomaterial-based
971 electrochemical biosensors for label-free sensing of environmental pollutants.
972 *Chemosphere* 143, 85–98

973 11. Pena-Pereira, F., Wojnowski, W., and Tobiszewski, M. (2020) AGREE - Analytical
974 GREEnness Metric Approach and Software. *Anal Chem* 92, 10076–10082

975 12. Pearson, J. E., Gill, A., and Vadgama, P. (2000) Analytical aspects of biosensors. *Ann*
976 *Clin Biochem* 37, 119–145

977 13. Malandain, C., Fayolle, F., and Bedouelle, H. (2005) Biosensors for the Environment. *Oil*
978 *& Gas Science and Technology* 60, 887–897

979 14. Bontidean, I., Berggren, C., Johansson, G., Csöregi, E., Mattiasson, B., Lloyd, J. R.,
980 Jakeman, K. J., and Brown, N. L. (1998) Detection of Heavy Metal Ions at Femtomolar
981 Levels Using Protein-Based Biosensors. *Anal Chem* 70, 4162–4169

982 15. Blake, D. A., Jones, R. M., Blake, R. C., Pavlov, A. R., Darwish, I. A., and Yu, H. (2001)
983 Antibody-based sensors for heavy metal ions. *Biosens Bioelectron* 16, 799–809

984 16. Chouteau, C., Dzyadevych, S., Durrieu, C., and Chovelon, J. M. (2005) A bi-enzymatic
985 whole cell conductometric biosensor for heavy metal ions and pesticides detection in
986 water samples. *Biosens Bioelectron* 21, 273–281

987 17. Mohammadi, Z. B., Zhang, F., Kharazmi, M. S., and Jafari, S. M. (2023) Nano-
988 biocatalysts for food applications; immobilized enzymes within different nanostructures.
989 *Crit Rev Food Sci Nutr* 63, 11351–11369

990 18. Sun, G., Wei, X., Zhang, D., Huang, L., Liu, H., and Fang, H. (2023) Immobilization of
991 Enzyme Electrochemical Biosensors and Their Application to Food Bioprocess
992 Monitoring. *Biosensors (Basel)* 13, 886

993 19. Kakkar, P., and Jaffery, F. N. (2005) Biological markers for metal toxicity. *Environ*
994 *Toxicol Pharmacol* 19, 335–349

995 20. Castillo, J., Gáspár, S., Leth, S., Niculescu, M., Mortari, A., Bontidean, I., Soukharev, V.,
996 Dorneanu, S. A., Ryabov, A. D., and Csöregi, E. (2004) Biosensors for life quality:
997 Design, development and applications. *Sens Actuators B Chem* 102, 179–194

998 21. Amaro, F., Turkewitz, A. P., Martín-González, A., and Gutiérrez, J. C. (2011) Whole-cell
999 biosensors for detection of heavy metal ions in environmental samples based on
1000 metallothionein promoters from Tetrahymena thermophila. *Microb Biotechnol* 4, 513–522

1001 22. Kim, Y., Choi, H., Shin, W. H., Oh, J. M., Koo, S. M., Kim, Y., Lee, T., Yu, B. J., and
1002 Park, C. (2021) Development of Colorimetric Whole-Cell Biosensor for Detection of
1003 Heavy Metals in Environment for Public Health. *International Journal of Environmental*
1004 *Research and Public Health 2021, Vol. 18, Page 12721* 18, 12721

1005 23. Bousse, L. (1996) Whole cell biosensors. *Sens Actuators B Chem* 34, 270–275

1006 24. Stenger, D. A., Gross, G. W., Keefer, E. W., Shaffer, K. M., Andreadis, J. D., Ma, W., and
1007 Pancrazio, J. J. (2001) Detection of physiologically active compounds using cell-based
1008 biosensors. *Trends Biotechnol* 19, 304–309

1009 25. Wang, Y.-Z., Christopher, J. K., Yong, Y.-C., and Zhai, D.-D. (2019) *Nutrient Detection*
1010 *with Whole-Cell Biosensors* (Springer, Cham)

1011 26. Mihaela, G., and Mihaela, G. (2021) A short review on cell-based biosensing: challenges
1012 and breakthroughs in biomedical analysis. *J Biomed Res* 35, 255–263

1013 27. Raut, N., O'Connor, G., Pasini, P., and Daunert, S. (2012) Engineered cells as biosensing
1014 systems in biomedical analysis. *Anal Bioanal Chem* 402, 3147–3159

1015 28. Gui, Q., Lawson, T., Shan, S., Yan, L., and Liu, Y. (2017) The Application of Whole Cell-
1016 Based Biosensors for Use in Environmental Analysis and in Medical Diagnostics. *Sensors*
1017 17, 1623

1018 29. Kannappan, S., Bhaskar, ·, Ramisetty, C. M., Chandra, B., and Ramisetty, M. (2021)
1019 Engineered Whole-Cell-Based Biosensors: Sensing Environmental Heavy Metal
1020 Pollutants in Water—a Review. *Applied Biochemistry and Biotechnology 2021 194:4* 194,
1021 1814–1840

1022 30. Kang, C., Shrestha, K. L., Kwon, S., Park, S., Kim, J., and Kwon, Y. (2022) Intein-
1023 Mediated Protein Engineering for Cell-Based Biosensors. *Biosensors (Basel)* 12, 283

1024 31. Jeon, H., Lee, E., Kim, D., Lee, M., Ryu, J., Kang, C., Kim, S., and Kwon, Y. (2018) Cell-
1025 Based Biosensors Based on Intein-Mediated Protein Engineering for Detection of
1026 Biologically Active Signaling Molecules. *Anal Chem* 90, 9779–9786

1027 32. Lee, E., Shrestha, K. L., Kang, S., Ramakrishnan, N., and Kwon, Y. (2023) Cell-Based
1028 Sensors for the Detection of EGF and EGF-Stimulated Ca2+ Signaling. *Biosensors*
1029 *(Basel)* 13, 383

1030 33. Jeon, H., Lee, M., Jang, W., and Kwon, Y. (2016) Intein-mediated protein engineering for
1031 biosensor fabrication. *Biochip J* 10, 277–287

1032 34. Mills, K. V., Johnson, M. A., and Perler, F. B. (2014) Protein Splicing: How Inteins
1033 Escape from Precursor Proteins. *Journal of Biological Chemistry* 289, 14498–14505

1034 35. Perler, F. B. (2005) Protein splicing mechanisms and applications. *IUBMB Life* 57, 469–
1035 476

1036 36. Panda, S., Nanda, A., Nasker, S. S., Sen, D., Mehra, A., and Nayak, S. (2021) Metal effect
1037 on intein splicing: A review. *Biochimie* 185, 53–67

1038 37. Nichols, N. M., Benner, J. S., Martin, D. D., and Evans, T. C. (2003) Zinc ion effects on
1039 individual Ssp DNaE intein splicing steps: Regulating pathway progression. *Biochemistry*
1040 42, 5301–5311

1041 38. Chan, H., Pearson, C. S., Green, C. M., Li, Z., Zhang, J., Belfort, G., Shekhtman, A., Li,
1042 H., and Belfort, M. (2016) Exploring Intein Inhibition by Platinum Compounds as an
1043 Antimicrobial Strategy. *Journal of Biological Chemistry* 291, 22661–22670

1044 39. Green, C. M., Li, Z., Smith, A. D., Novikova, O., Bacot-Davis, V. R., Gao, F., Hu, S.,
1045 Banavali, N. K., Thiele, D. J., Li, H., and Belfort, M. (2019) Spliceosomal Prp8 intein at
1046 the crossroads of protein and RNA splicing. *PLoS Biol* 17, e3000104

1047 40. Ojha, D. K., Mehra, A., Rout, S. S., Giri, S., and Nayak, S. (2025) Bactericidal activity of
1048 ZnO nanoparticles–anti-TB drug combination towards the H37Rv strain and multidrug-
1049 resistant isolates of Mycobacterium tuberculosis via SufB splicing inhibition. *Mater Adv*
1050 6, 5242–5259

1051 41. Gramespacher, J. A., Stevens, A. J., Nguyen, D. P., Chin, J. W., and Muir, T. W. (2017)
1052 Intein Zymogens: Conditional Assembly and Splicing of Split Inteins via Targeted
1053 Proteolysis. *J Am Chem Soc* 139, 8074–8077

1054 42. Skretas, G., and Wood, D. W. (2005) Regulation of protein activity with small-molecule-
1055 controlled inteins. *Protein Science* 14, 523–532

1056 43. Panda, S., Nanda, A., Nasker, S. S., Mehra, A., Ojha, D. K., Mohanty, P. S., and Nayak, S.
1057 (2023) Metal regulation of Mycobacterium tuberculosis SufB intein splicing at the host–
1058 pathogen crossroad. *Clin Sci* 137, 1027–1048

1059 44. Poland, B. W., Xu, M. Q., and Quiocho, F. A. (2000) Structural Insights into the Protein
1060 Splicing Mechanism of PI-SceI. *Journal of Biological Chemistry* 275, 16408–16413

1061 45. Mills, K. V., and Paulus, H. (2001) Reversible Inhibition of Protein Splicing by Zinc Ion.
1062 *Journal of Biological Chemistry* 276, 10832–10838

1063 46. Van Roey, P., Pereira, B., Li, Z., Hiraga, K., Belfort, M., and Derbyshire, V. (2007)
1064 Crystallographic and Mutational Studies of Mycobacterium tuberculosis recA Mini-inteins
1065 Suggest a Pivotal Role for a Highly Conserved Aspartate Residue. *J Mol Biol* 367, 162–
1066 173

1067 47. Zhang, L., Zheng, Y., Xi, Z., Luo, Z., Xu, X., Wang, C., and Liu, Y. (2009) Metal ions
1068 binding to recA inteins from Mycobacterium tuberculosis. *Mol Biosyst* 5, 644–650

1069 48. Sun, P., Ye, S., Ferrandon, S., Evans, T. C., Xu, M. Q., and Rao, Z. (2005) Crystal
1070 Structures of an Intein from the Split dnaE Gene of Synechocystis sp. PCC6803 Reveal

1071 the Catalytic Model Without the Penultimate Histidine and the Mechanism of Zinc Ion
1072 Inhibition of Protein Splicing. *J Mol Biol* 353, 1093–1105

1073 49. Woods, D., Vangaveti, S., Egbanum, I., Sweeney, A. M., Li, Z., Bacot-Davis, V.,
1074 Lesassier, D. S., Stanger, M., Hardison, G. E., Li, H., Belfort, M., and Lennon, C. W.
1075 (2020) Conditional DnaB protein splicing is reversibly inhibited by zinc in mycobacteria.
1076 *mBio* 11, 1–14

1077 50. Pearson, C. S., Belfort, G., Belfort, M., and Shekhtman, A. (2015) Backbone assignments
1078 of mini-RecA intein with short native exteins and an active N-terminal catalytic cysteine.
1079 *Biomol NMR Assign* 9, 235–238

1080 51. Li, Z., Fu, B., Green, C. M., Liu, B., Zhang, J., Lang, Y., Chaturvedi, S., Belfort, M., Liao,
1081 G., and Li, H. (2019) Cisplatin protects mice from challenge of Cryptococcus neoformans
1082 by targeting the Prp8 intein. *Emerg Microbes Infect* 8, 895–908

1083 52. Ozawa, T., Nogami, S., Sato, M., Ohya, Y., and Umezawa, Y. (2000) A Fluorescent
1084 Indicator for Detecting Protein−Protein Interactions in Vivo Based on Protein Splicing.
1085 *Anal Chem* 72, 5151–5157

1086 53. Ozawa, T., Kaihara, A., Sato, M., Tachihara, K., and Umezawa, Y. (2001) Split
1087 Luciferase as an Optical Probe for Detecting Protein−Protein Interactions in Mammalian
1088 Cells Based on Protein Splicing. *Anal Chem* 73, 2516–2521

1089 54. Paulmurugan, R., Umezawa, Y., and Gambhir, S. S. (2002) Noninvasive imaging of
1090 protein–protein interactions in living subjects by using reporter protein complementation
1091 and reconstitution strategies. *Proceedings of the National Academy of Sciences* 99,
1092 15608–15613

1093 55. Kanno, A., Ozawa, T., and Umezawa, Y. (2005) Intein-Mediated Reporter Gene Assay for
1094 Detecting Protein−Protein Interactions in Living Mammalian Cells. *Anal Chem* 78, 556–
1095 560

1096 56. Topilina, N. I., Green, C. M., Jayachandran, P., Kelley, D. S., Stanger, M. J., Piazza, C.
1097 L., Nayak, S., and Belfort, M. (2015) SufB intein of Mycobacterium tuberculosis as a
1098 sensor for oxidative and nitrosative stresses. *Proc Natl Acad Sci U S A* 112, 10348–10353

1099 57. Zhang, L., Xiao, N., Pan, Y., Zheng, Y., Pan, Z., Luo, Z., Xu, X., and Liu, Y. (2010)
1100 Binding and inhibition of copper ions to RecA inteins from mycobacterium tuberculosis.
1101 *Chemistry - A European Journal* 16, 4297–4306

1102 58. Zhang, L., Zheng, Y., Callahan, B., Belfort, M., and Liu, Y. (2011) Cisplatin Inhibits
1103 Protein Splicing, Suggesting Inteins as Therapeutic Targets in Mycobacteria. *Journal of*
1104 *Biological Chemistry* 286, 1277–1282

1105 59. Dassa, B., Amitai, G., Caspi, J., Schueler-Furman, O., and Pietrokovski, S. (2007) Trans
1106 protein splicing of cyanobacterial split inteins in endogenous and exogenous
1107 combinations. *Biochemistry* 46, 322–330

1108 60. Huet, G., Daffé, M., and Saves, I. (2005) Identification of the Mycobacterium tuberculosis
1109 SUF machinery as the exclusive mycobacterial system of [Fe-S] cluster assembly:
1110 Evidence for its implication in the pathogen's survival. *J Bacteriol* 187, 6137–6146

1111 61. Huet, G., Castaing, J. P., Fournier, D., Daffé, M., and Saves, I. (2006) Protein splicing of
1112 SufB is crucial for the functionality of the Mycobacterium tuberculosis SUF machinery. *J*
1113 *Bacteriol* 188, 3412–3414

1114 62. Panda, S., Nanda, A., Sahu, N., Ojha, D. K., Pradhan, B., Rai, A., Suryawanshi, A. R.,
1115 Banavali, N., and Nayak, S. (2022) SufB intein splicing in Mycobacterium tuberculosis is
1116 influenced by two remote conserved N-extein histidines. *Biosci Rep* 42, 20212207

1117 63. Friedel, K., Popp, M. A., Matern, J. C. J., Gazdag, E. M., Thiel, I. V., Volkmann, G.,
1118 Blankenfeldt, W., and Mootz, H. D. (2018) A functional interplay between intein and
1119 extein sequences in protein splicing compensates for the essential block B histidine. *Chem*
1120 *Sci* 10, 239–251

1121 64. Kelley, D. S., Lennon, C. W., Li, Z., Miller, M. R., Banavali, N. K., Li, H., and Belfort,
1122 M. (2018) Mycobacterial DnaB helicase intein as oxidative stress sensor. *Nat Commun* 9,
1123 1–15

1124 65. Mills, K. V., Lew, B. M., Jiang, S. Q., and Paulus, H. (1998) Protein splicing in trans by
1125 purified N- and C-terminal fragments of the Mycobacterium tuberculosis RecA intein.
1126 *Proc Natl Acad Sci U S A* 95, 3543–3548

1127 66. Gangopadhyay, J. P., Jiang, S. qin, and Paulus, H. (2003) An in vitro screening system for
1128 protein splicing inhibitors based on green fluorescent protein as an indicator. *Anal Chem*
1129 75, 2456–2462

1130 67. Nanda, A., Nasker, S. S., Kushwaha, A. K., Ojha, D. K., Dearden, A. K., Nayak, S. K.,
1131 and Nayak, S. (2021) Gold Nanoparticles Augment N-Terminal Cleavage and Splicing
1132 Reactions in Mycobacterium tuberculosis SufB. *Front Bioeng Biotechnol* 9, 773303

1133 68. Chemiluminescence, B., Li, J., Xing, H., Wang, E., Zhao, J., Li, D., Ma, J., Suhartono, E.,
1134 Thalib, I., Aflanie, I., Noor, Z., and Idroes, R. (2018) in *IOP Conference Series: Materials*
1135 *Science and Engineering* (IOP Publishing), p 012008.

1136 69. Grzyska, P. K., Hausinger, R. P., and Proshlyakov, D. A. (2010) Metal and substrate
1137 binding to an Fe(II) dioxygenase resolved by UV spectroscopy with global regression
1138 analysis. *Anal Biochem* 399, 64–71

1139 70. Plotnikova, O. A., Mel'nikov, A. G., Mel'nikov, G. V., and Gubina, T. I. (2016)
1140 Quenching of tryptophan fluorescence of bovine serum albumin under the effect of ions of
1141 heavy metals. *Opt Spectrosc* 120, 65–69

1142 71. Oliveira, A., Baccana, N., and Cadore, S. (2012) Evaluation of metal ions in rice samples:
1143 extraction and direct determination by ICP OES. *J Braz Chem Soc* 23, 838–845

1144 72. Harrington, J. M., Young, D. J., Essader, A. S., Sumner, S. J., and Levine, K. E. (2014)
1145 Analysis of human serum and whole blood for mineral content by ICP-MS and ICP-OES:
1146 Development of a mineralomics method. *Biol Trace Elem Res* 160, 132–142

1147 73. Punjabi, K., Mehta, S., Chavan, R., Chitalia, V., Deogharkar, D., and Deshpande, S.
1148 (2018) Efficiency of biosynthesized silver and zinc nanoparticles against multi-drug
1149 resistant pathogens. *Front Microbiol* 9, 376058

1150 74. Longhin, E. M., El Yamani, N., Rundén-Pran, E., and Dusinska, M. (2022) The alamar
1151 blue assay in the context of safety testing of nanomaterials. *Frontiers in Toxicology* 4,
1152 981701

1153 75. Yang, L., Zhang, Y., Wang, F., Luo, Z., Guo, S., and Strähle, U. (2020) Toxicity of
1154 mercury: Molecular evidence. *Chemosphere* 245, 125586

1155 76. Aljerf, L., Almasri, N., and Access, O. (2018) Mercury toxicity: ecological features of
1156 organic phase of mercury in biota-Part I. *Inorganic Chemical Sciences* 3,

1157 77. Budnik, L. T., and Casteleyn, L. (2019) Mercury pollution in modern times and its socio-
1158 medical consequences. *Science of The Total Environment* 654, 720–734

1159 78. Dash, H. R., Mangwani, N., and Das, S. (2014) Characterization and potential application
1160 in mercury bioremediation of highly mercury-resistant marine bacterium Bacillus
1161 thuringiensis PW-05. *Environmental Science and Pollution Research* 21, 2642–2653

1162 79. Tang, W., Zhang, W., Zhao, Y., Zhang, H., and Shan, B. (2017) Basin-scale
1163 comprehensive assessment of cadmium pollution, risk, and toxicity in riverine sediments
1164 of the Haihe Basin in north China. *Ecol Indic* 81, 295–301

1165 80. White, P. J., and Brown, P. H. (2010) Plant nutrition for sustainable development and
1166 global health. *Ann Bot* 105, 1073–1080

1167 81. Losada Ros, M. T., Al-Enezi, E., Cesarini, E., Canonico, B., Bucci, C., Martins, M. V. A.,
1168 Papa, S., and Frontalini, F. (2020) Assessing the Cadmium Effects on the Benthic
1169 Foraminifer Ammonia cf. parkinsoniana: An Acute Toxicity Test. *Water (Basel)* 12, 1018

1170 82. Dong, F., Zhu, X., Qian, W., Wang, P., and Wang, J. (2020) Combined effects of CO2-
1171 driven ocean acidification and Cd stress in the marine environment: Enhanced tolerance of
1172 Phaeodactylum tricornutum to Cd exposure. *Mar Pollut Bull* 150, 110594

1173 83. Atamaleki, A., Sadani, M., Raoofi, A., Miri, A., Bajestani, S. G., Fakhri, Y., Heidarinejad,
1174 Z., and Mousavi Khaneghah, A. (2020) The concentration of potentially toxic elements
1175 (PTEs) in eggs: A global systematic review, meta-analysis and probabilistic health risk
1176 assessment. *Trends Food Sci Technol* 95, 1–9

1177 84. Stankovic, S., Kalaba, P., and Stankovic, A. R. (2014) Biota as toxic metal indicators.
1178 *Environ Chem Lett* 12, 63–84

1179 85. Joe, M. H., Lee, K. H., Lim, S. Y., Im, S. H., Song, H. P., Lee, I. S., and Kim, D. H.
1180 (2012) Pigment-based whole-cell biosensor system for cadmium detection using
1181 genetically engineered Deinococcus radiodurans. *Bioprocess Biosyst Eng* 35, 265–272

1182 86. Guertin, J., Jacobs, J. A., and Avakian, C. P. (2004) *Chromium(VI) Handbook* (CRC
1183 Press). 1st Ed.

1184 87. Dawra, N., and Dabas, N. (2024) Advances in spectrophotometric determination of
1185 Chromium(III) and Chromium(VI) in water: a review. *Int J Environ Anal Chem* 104,
1186 2994–3015

1187 88. Sheehan, P. J., Meyer, D. M., Sauer, M. M., and Paustenbach, D. J. (1991) Assessment of
1188 the human health risks posed by exposure to chromium-contaminated soils. *Journal of*
1189 *Toxicology and Environmental Health, Part A Current Issues* 32, 161–201

1190 89. Mishra, S., and Bharagava, R. N. (2016) Toxic and genotoxic effects of hexavalent
1191 chromium in environment and its bioremediation strategies. *Journal of Environmental*
1192 *Science and Health, Part C* 34, 1–32

1193 90. Feleafel, M. N., and Mirdad, Z. M. (2013) Hazard and Effects of Pollution by Lead on
1194 Vegetable Crops. *J Agric Environ Ethics* 26, 547–567

1195 91. Ghosh, I., Sun, L., and Xu, M. Q. (2001) Zinc Inhibition of Protein trans-Splicing and
1196 Identification of Regions Essential for Splicing and Association of a Split Intein*. *Journal*
1197 *of Biological Chemistry* 276, 24051–24058

1198 92. Tharappel, A. M., Li, Z., and Li, H. (2022) Inteins as Drug Targets and Therapeutic Tools.
1199 *Front Mol Biosci* 9, 821146

1200 93. Alhazmi, H. A., Alam, M. S., Albratty, M., Najmi, A., Abdulhaq, A. A., Hassani, R.,
1201 Ahsan, W., and Qramish, A. N. (2023) Binding Investigation of Some Important Metal
1202 Ions Copper (I), Nickel (II), and Aluminium (III) with Bovine Serum Albumin Using
1203 Valid Spectroscopic Techniques. *J Chem* 2023, 2581653

1204 94. Permyakov, E. A., and Gonçalves, A. M. M. (2021) Metal Binding Proteins. *Encyclopedia*
1205 1, 261–292

1206 95. Woźnicka, O., Rybarska, J., Jagusiak, A., Konieczny, L., Stopa, B., and Roterman, I.
1207 (2017) Metal ions introduced to proteins by supramolecular ligands. *Self-Assembled*
1208 *Molecules - New Kind of Protein Ligands: Supramolecular Ligands*, 61–76

1209 96. Antosiewicz, J. M., and Shugar, D. (2016) UV–Vis spectroscopy of tyrosine side-groups
1210 in studies of protein structure. Part 2: selected applications. *Biophys Rev* 8, 163–177

1211 97. Biter, A. B., Pollet, J., Chen, W. H., Strych, U., Hotez, P. J., and Bottazzi, M. E. (2019) A
1212 method to probe protein structure from UV absorbance spectra. *Anal Biochem* 587,
1213 113450

1214 98. Dieaconu, M., Ioanid, A., Iftimie, S., and Antohe, S. UV-ABSORPTION MECHANISMS
1215 OF Ni 2+-BINDING BOVINE SERUM ALBUMIN. *Dig J Nanomater Biostruct* 7, 1125–
1216 1138

1217 99. View of Study of immunoglobulin 'G' with ultra violet spectroscopy in Duchene muscular
1218 dystrophy and Alzheimer's disease

1219 100. Bjørklund, G., Dadar, M., Mutter, J., and Aaseth, J. (2017) The toxicology of mercury:
1220 Current research and emerging trends. *Environ Res* 159, 545–554

1221 101. Ajsuvakova, O. P., Tinkov, A. A., Aschner, M., Rocha, J. B. T., Michalke, B., Skalnaya,
1222 M. G., Skalny, A. V., Butnariu, M., Dadar, M., Sarac, I., Aaseth, J., and Bjørklund, G.
1223 (2020) Sulfhydryl groups as targets of mercury toxicity. *Coord Chem Rev* 417, 213343

1224 102. Sall, M. L., Diaw, A. K. D., Gningue-Sall, D., Efremova Aaron, S., and Aaron, J. J. (2020)
1225 Toxic heavy metals: impact on the environment and human health, and treatment with
1226 conducting organic polymers, a review. *Environmental Science and Pollution Research*
1227 27, 29927–29942

1228 103. Gonick, H. C. (2011) Lead-Binding Proteins: A Review. *J Toxicol* 2011, 686050

1229 104. Fossum, C. J., Johnson, B. O. V., Golde, S. T., Kielman, A. J., Finke, B., Smith, M. A.,
1230 Lowater, H. R., Laatsch, B. F., Bhattacharyya, S., and Hati, S. (2023) Insights into the
1231 Mechanism of Tryptophan Fluorescence Quenching due to Synthetic Crowding Agents: A
1232 Combined Experimental and Computational Study. *ACS Omega* 8, 44820–44830

1233 105. Liu, Y., Xu, J., Han, L., Liu, Q., Yang, Y., Li, Z., Lu, Z., Zhang, H., Guo, T., and Liu, Q.
1234 (2020) Theoretical Research on Excited States: Ultraviolet and Fluorescence Spectra of
1235 Aromatic Amino Acids. *Interdiscip Sci* 12, 530–536

1236 106. Yammine, A., Gao, J., and Kwan, A. H. (2019) Tryptophan Fluorescence Quenching
1237 Assays for Measuring Protein-ligand Binding Affinities: Principles and a Practical Guide.
1238 *Bio Protoc* 9,

1239 107. Zheng, Z., Kawakami, K., Zhang, D., Negishi, L., Abomosallam, M., Asakura, T., Nagata,
1240 K., and Suzuki, M. (2021) Identification and functional analysis of cadmium-binding
1241 protein in the visceral mass of Crassostrea gigas. *Sci Rep* 11, 1–14

1242 108. Springfield, E., Willis, A., Merle, J., Mazlo, J., and Ngu-Schwemlein, M. (2021)
1243 Spectroscopic and Theoretical Studies of Hg(II) Complexation with Some Dicysteinyl
1244 Tetrapeptides. *Bioinorg Chem Appl* 2021, 9911474

1245 109. Crouse, H. F., Petrunak, E. M., Donovan, A. M., Merkle, A. C., Swartz, B. L., and Basu,
1246 S. (2011) Static and dynamic quenching of tryptophan fluorescence in various proteins by
1247 a chromium (III) complex. *Spectroscopy Letters* 44, 369–374

1248 110. Shrivastava, H. Y., and Nair, B. U. (2004) Fluorescence resonance energy transfer from
1249 tryptophan to a chromium(III) complex accompanied by non-specific cleavage of
1250 albumin: a step forward towards the development of a novel photoprotease. *J Inorg*
1251 *Biochem* 98, 991–994

1252 111. Liu, Y., Zhang, L., Liu, R., and Zhang, P. (2012) Spectroscopic identification of
1253 interactions of Pb 2+ with bovine serum albumin. *J Fluoresc* 22, 239–245

1254 112. Gen-hua Wu Study on the interaction of Pb2+ and bovine serum albumin by fluorescence.

1255 113. Luis, G., Rubio, C., Revert, C., Espinosa, A., González-Weller, D., Gutiérrez, A. J., and
1256 Hardisson, A. (2015) Dietary intake of metals from yogurts analyzed by inductively
1257 coupled plasma optical emission spectrometry (ICP-OES). *Journal of Food Composition*
1258 *and Analysis* 39, 48–54

1259 114. Wiltsche, H., and Wolfgang, M. (2020) Merits of microwave plasmas for optical emission
1260 spectrometry – characterization of an axially viewed microwave-sustained, inductively
1261 coupled, atmospheric-pressure plasma (MICAP). *J Anal At Spectrom* 35, 2369–2377

1262 115. Baraud, F., Zaiter, A., Porée, S., and Leleyter, L. (2020) New approach for determination
1263 of Cd, Cu, Cr, Ni, Pb, and Zn in sewage sludges, fired brick, and sediments using two
1264 analytical methods by microwave-induced plasma optical spectrometry and induced
1265 coupled plasma optical spectrometry. *SN Appl Sci* 2, 1–10

1266 116. Wegener Antje, Marc Wiesmann, Peter Luschas, Kerstin Vogel, and Matthias Pursch
1267 (2019) SEC-ICP-OES Hyphenation: Speciation and Quantification of
1268 Polydimethylsiloxanes at Trace levels. *Spectroscopy*, 38–46

1269 117. Pandey, M., Talwar, S., Bose, S., and Pandey, A. K. (2018) Iron homeostasis in
1270 Mycobacterium tuberculosis is essential for persistence. *Sci Rep* 8, 1–9

1271 118. Tripathi, A., Anand, K., Das, M., O'Niel, R. A., Sabarinath, P. S., Thakur, C., Reddy, R.
1272 R. L., Rajmani, R. S., Chandra, N., Laxman, S., and Singh, A. (2022) Mycobacterium
1273 tuberculosis requires SufT for Fe-S cluster maturation, metabolism, and survival in vivo.
1274 *PLoS Pathog* 18, e1010475

1275 119. Saini, V., Farhana, A., Glasgow, J. N., and Steyn, A. J. C. (2012) Iron sulfur cluster
1276 proteins and microbial regulation: implications for understanding tuberculosis. *Curr Opin*
1277 *Chem Biol* 16, 45–53

1278 120. Wang, P., Xu, G., Qin, L., Xu, Y., Li, Y., and Li, R. (2005) Cell-based biosensors and its
1279 application in biomedicine. *Sens Actuators B Chem* 108, 576–584

1280 121. Gupta, N., Renugopalakrishnan, V., Liepmann, D., Paulmurugan, R., and Malhotra, B. D.
1281 (2019) Cell-based biosensors: Recent trends, challenges and future perspectives. *Biosens*
1282 *Bioelectron* 141, 111435

1283 122. Perler, F. B. (2002) InBase: the Intein Database. *Nucleic Acids Res* 30, 383–384

1284 123. Yakovleva, L., and Shuman, S. (2012) Mycobacterium smegmatis SftH exemplifies a
1285 distinctive clade of superfamily II DNA-dependent ATPases with 3′ to 5′ translocase and
1286 helicase activities. *Nucleic Acids Res* 40, 7465–7475

1287 124. Ordonez, H., and Shuman, S. (2013) Mycobacterium smegmatis Lhr Is a DNA-dependent
1288 ATPase and a 3′-to-5′ DNA Translocase and Helicase That Prefers to Unwind 3′-Tailed
1289 RNA:DNA Hybrids. *Journal of Biological Chemistry* 288, 14125–14134

1290 125. Uson, M. L., Ordonez, H., and Shuman, S. (2015) Mycobacterium smegmatis HelY Is an
1291 RNA-Activated ATPase/dATPase and 3′-to-5′ Helicase That Unwinds 3′-Tailed RNA
1292 Duplexes and RNA:DNA Hybrids. *J Bacteriol* 197, 3057–3065

1293 126. Rampersad, S. N. (2012) Multiple Applications of Alamar Blue as an Indicator of
1294 Metabolic Function and Cellular Health in Cell Viability Bioassays. *Sensors* 12, 12347–
1295 12360

1296 127. O'Brien, J., Wilson, I., Orton, T., and Pognan, F. (2000) Investigation of the Alamar Blue
1297 (resazurin) fluorescent dye for the assessment of mammalian cell cytotoxicity. *Eur J*
1298 *Biochem* 267, 5421–5426

1299 128. McMillan, J. E. (2013) *Principles of Analytical Validation* (Elsevier Inc.)

1300 129. Howard, J. A., Kuznietsova, H., Dziubenko, N., Aigle, A., Natuzzi, M., Thomas, E.,
1301 Lysenko, V., David, L., Brichart, T., Lux, F., and Tillement, O. (2023) Combating lead

1302 and cadmium exposure with an orally administered chitosan-based chelating polymer. *Sci*
1303 *Rep* 13, 1–14

1304 130. Saleh, S. M., El-Tawil, O. S., Mahmoud, M. B., Abd El-Rahman, S. S., El-Saied, E. M.,
1305 and Noshy, P. A. (2024) Do Nanoparticles of Calcium Disodium EDTA Minimize the
1306 Toxic Effects of Cadmium in Female Rats? *Biol Trace Elem Res* 202, 2228–2240

1307 131. Flora, S. J. S., and Pachauri, V. (2010) Chelation in Metal Intoxication. *Int J Environ Res*
1308 *Public Health* 7, 2745–2788

1309 132. Bethesda (2012) *LiverTox* (National Institute of Diabetes and Digestive and Kidney
1310 Diseases)

1311 133. George, G. N., Prince, R. C., Gailer, J., Buttigieg, G. A., Denton, M. B., Harris, H. H., and
1312 Pickering, I. J. (2004) Mercury binding to the chelation therapy agents DMSA and DMPS
1313 and the rational design of custom chelators for mercury. *Chem Res Toxicol* 17, 999–1006

1314 134. Aaseth, J., Ajsuvakova, O. P., Skalny, A. V., Skalnaya, M. G., and Tinkov, A. A. (2018)
1315 Chelator combination as therapeutic strategy in mercury and lead poisonings. *Coord Chem*
1316 *Rev* 358, 1–12

1317 135. Martí-Baena, Q., Pascuet-Fontanet, A., Berjaga-Buisan, T., Caravaca-Rodríguez, M.,
1318 Puig-Costa-Jussà, J., Sanchez-Mejias, A., Ivančić, D., Mogas-Díez, S., Güell, M., and
1319 Macia, J. (2024) Intein-mediated thyroid hormone biosensors: towards controlled delivery
1320 of hormone therapy. *Frontiers in Systems Biology* 4, 1270071

1321 136. Chahal, H. K., Dai, Y., Saini, A., Ayala-Castro, C., and Outten, F. W. (2009) The SufBCD
1322 Fe−S Scaffold Complex Interacts with SufA for Fe−S Cluster Transfer. *Biochemistry* 48,
1323 10644–10653

1324 137. Zhang, L., Xiao, N., Pan, Y., Zheng, Y., Pan, Z., Luo, Z., Xu, X., and Liu, Y. (2010)
1325 Binding and Inhibition of Copper Ions to RecA Inteins from Mycobacterium tuberculosis.
1326 *Chemistry – A European Journal* 16, 4297–4306

1327 138. Shaloam R, D. (2015) Preclinical Assessment of Low Doses of Cisplatin in the
1328 Management of Acute Promyelocytic Leukemia. *Int J Cancer Res Mol Mech* 1,

1329 139. Lennon, C. W., Wahl, D., Goetz, J. R., and Joel Weinberger, I. (2021) Reactive Chlorine
1330 Species Reversibly Inhibit DnaB Protein Splicing in Mycobacteria. *Microbiol Spectr* 9,

1331 140. Dillon, N. A., Lamont, E. A., Rather, M. A., and Baughn, A. D. (2025) Oxidative stress
1332 drives potent bactericidal activity of pyrazinamide against Mycobacterium tuberculosis.
1333 *Elife* 14,

141. Zhang, M., Gong, J., Lin, Y., and Barnes, P. F. (1998) Growth of Virulent and AvirulentMycobacterium tuberculosis Strains in Human Macrophages. *Infect Immun* 66, 794–799

142. Revised National TB Control Programme Training Manual for Mycobacterium tuberculosis

143. Davis, E. O., Sedgwick, S. G., and Colston, M. J. (1991) Novel structure of the recA locus of Mycobacterium tuberculosis implies processing of the gene product. *J Bacteriol* 173, 5653–5662

144. Saves, I., Westrelin, F., Daffé, M., and Masson, J. M. (2001) Identification of the first eubacterial endonuclease coded by an intein allele in the pps1 gene of mycobacteria. *Nucleic Acids Res* 29, 4310–4318

145. Schneider, R. F., Hallstrom, K., DeMott, C., and McDonough, K. A. (2024) Conditional protein splicing of the Mycobacterium tuberculosis RecA intein in its native host. *Sci Rep* 14, 1–14

A.

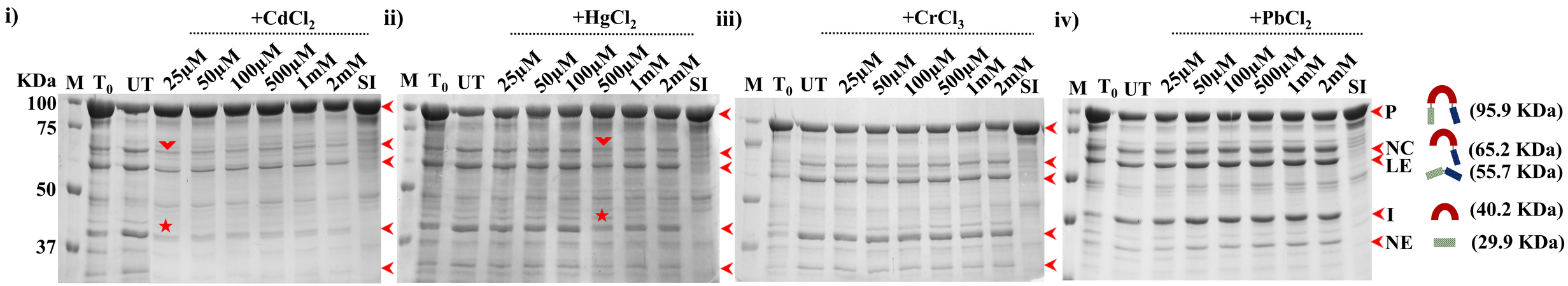
i)
+CdCl2
ii)
+HgCl2
iii)
+CrCl3
iv)
+PbCl2
KDa
M T0 UT 25µM 50µM 100µM 500µM 1mM 2mM SI
100
75
50
37
P
NC
LE
I
NE
(95.9 KDa)
(65.2 KDa)
(55.7 KDa)
(40.2 KDa)
(29.9 KDa)

B.

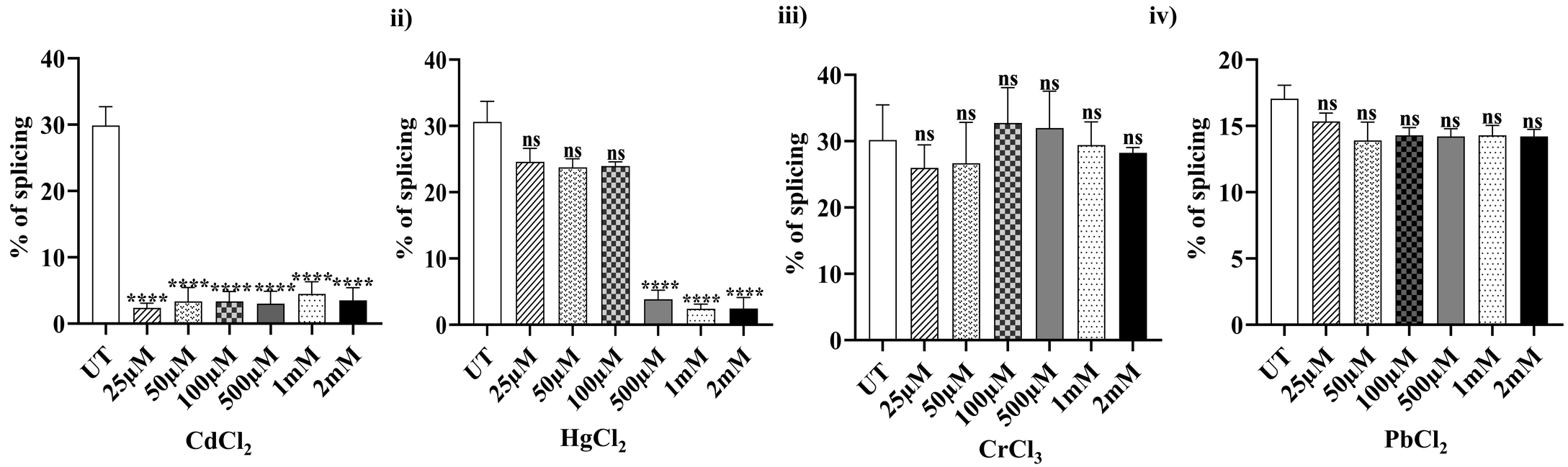
i)
ii)
iii)
iv)
% of splicing
UT 25µM 50µM 100µM 500µM 1mM 2mM
CdCl2
HgCl2
CrCl3
PbCl2
****
ns

C.

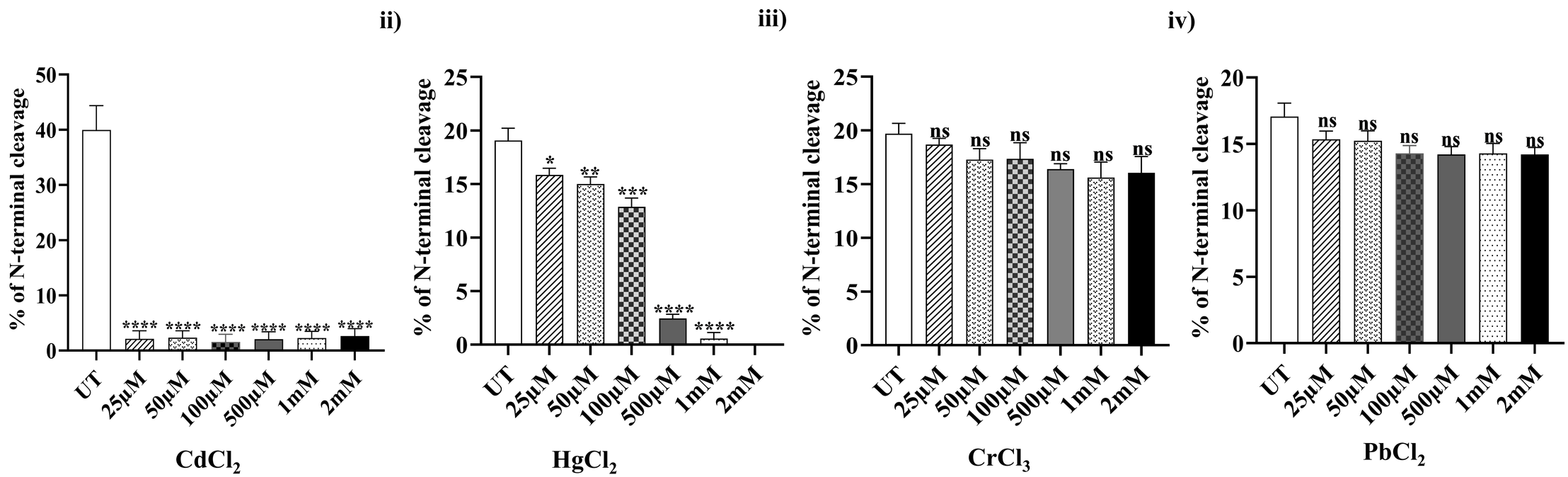
i)
ii)
iii)
iv)
% of N-terminal cleavage
UT 25µM 50µM 100µM 500µM 1mM 2mM
CdCl2
HgCl2
CrCl3
PbCl2
****
*
**
***
ns

i)

$Cd^{2+}$ | $Hg^{2+}$

H37Ra | *M. sm* | H37Ra | *M. sm*

| | | | | | | | | | |
|---|---|---|---|---|---|---|---|---|---|
| Cd 2.5 µM | Cd 25 µM | Cd 100 µM | Cd 1 mM | *M.Sm* +Cd 25 µM | Hg 25 µM | Hg 100 µM | Hg 1 mM | *M.Sm* + Hg 25 µM | +ve control |
| Cd 2.5 µM | Cd 25 µM | Cd 100 µM | Cd 1 mM | *M.Sm* +Cd 25 µM | Hg 25 µM | Hg 100 µM | Hg 1 mM | *M.Sm* + Hg 25 µM | +ve control |
| Cd 5 µM | Cd 25 µM | Cd 100 µM | Cd 1 mM | *M.Sm* +Cd 500 µM | Hg 25 µM | Hg 100 µM | Hg 1 mM | *M.Sm* +Hg 500 µM | +ve control |
| Cd 5 µM | Cd 50 µM | Cd 500 µM | Cd 2 mM | *M.Sm* +Cd 500 µM | Hg 50 µM | Hg 500 µM | Hg 2 mM | *M.Sm* +Hg 500 µM | -ve control |
| Cd 10 µM | Cd 50 µM | Cd 500 µM | Cd 2 mM | *M.Sm* +Cd 2 mM | Hg 50 µM | Hg 500 µM | Hg 2 mM | *M.Sm* + Hg 2 mM | -ve control |
| Cd 10 µM | Cd 50 µM | Cd 500 µM | Cd 2 mM | *M.Sm* +Cd 2 mM | Hg 50 µM | Hg 500 µM | Hg 2 mM | *M.Sm* + Hg 2 mM | -ve control |

+ve control

-ve control

ii)

$Cd^{2+}$ | $Hg^{2+}$

H37Ra | *M. sm* | H37Ra | *M. sm*

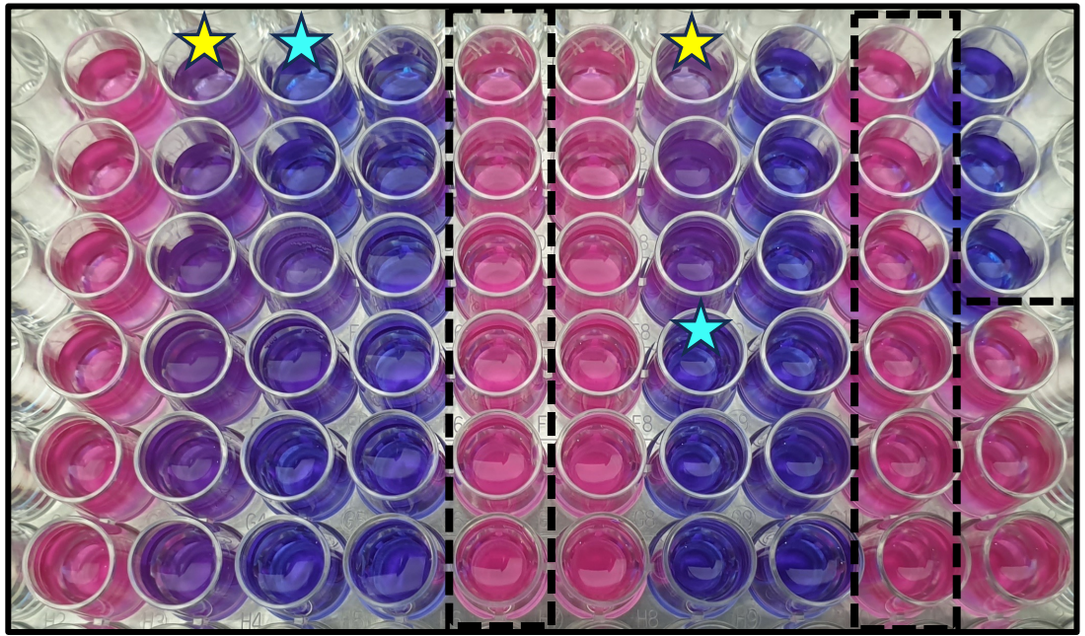

+ve control

-ve control

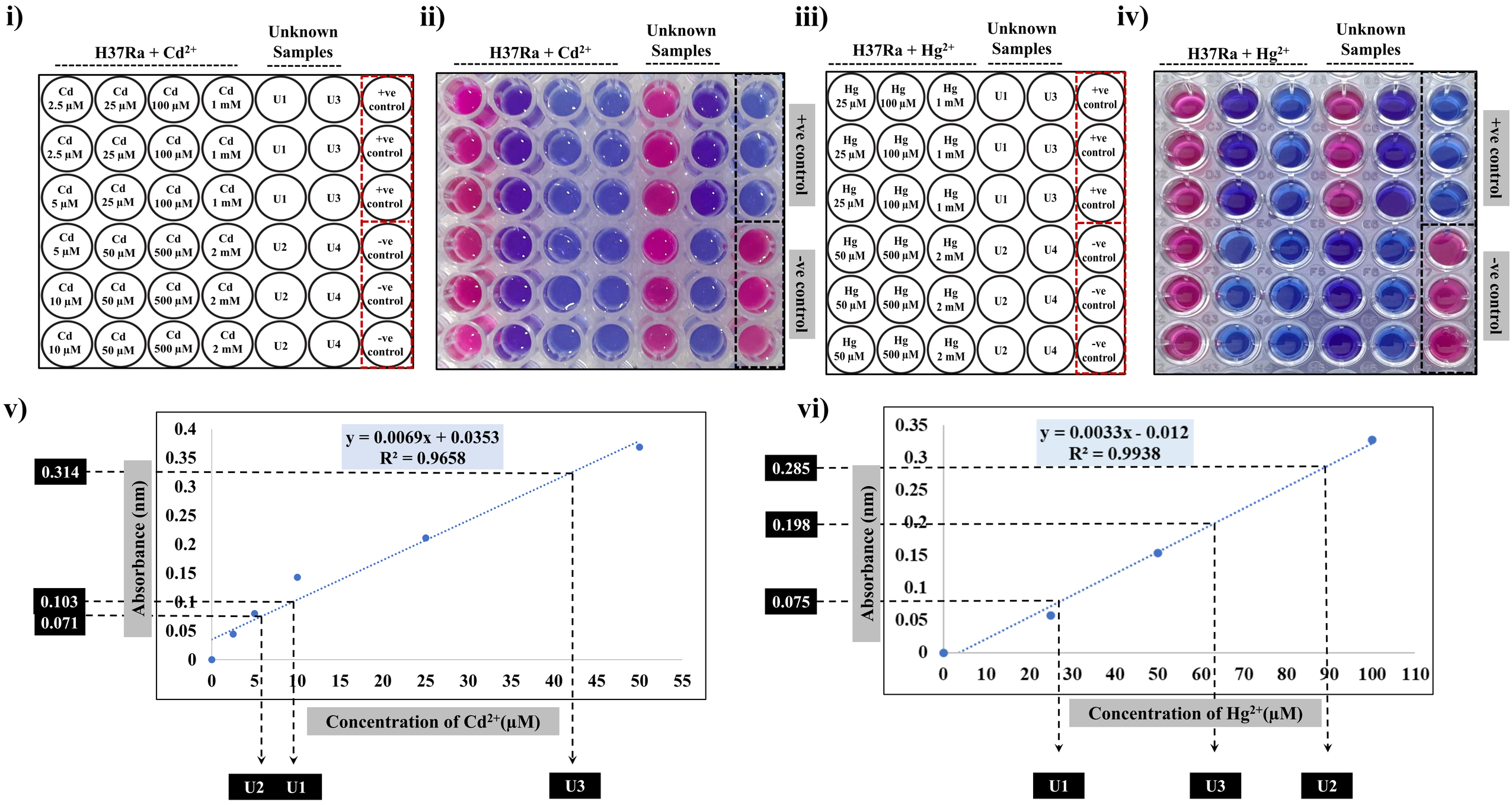
i)
H37Ra + Cd2+
Unknown Samples
Cd 2.5 µM
Cd 25 µM
Cd 100 µM
Cd 1 mM
U1
U3
+ve control
Cd 5 µM
Cd 50 µM
Cd 500 µM
Cd 2 mM
U2
U4
-ve control
Cd 10 µM
ii)
H37Ra + Cd2+
Unknown Samples
+ve control
-ve control
iii)
H37Ra + Hg2+
Unknown Samples
Hg 25 µM
Hg 100 µM
Hg 1 mM
Hg 50 µM
Hg 500 µM
Hg 2 mM
iv)
H37Ra + Hg2+
Unknown Samples
+ve control
-ve control
v)
y = 0.0069x + 0.0353
R² = 0.9658
Absorbance (nm)
0.314
0.103
0.071
Concentration of Cd2+(µM)
U2
U1
U3
vi)
y = 0.0033x - 0.012
R² = 0.9938
Absorbance (nm)
0.285
0.198
0.075
Concentration of Hg2+(µM)
U1
U3
U2

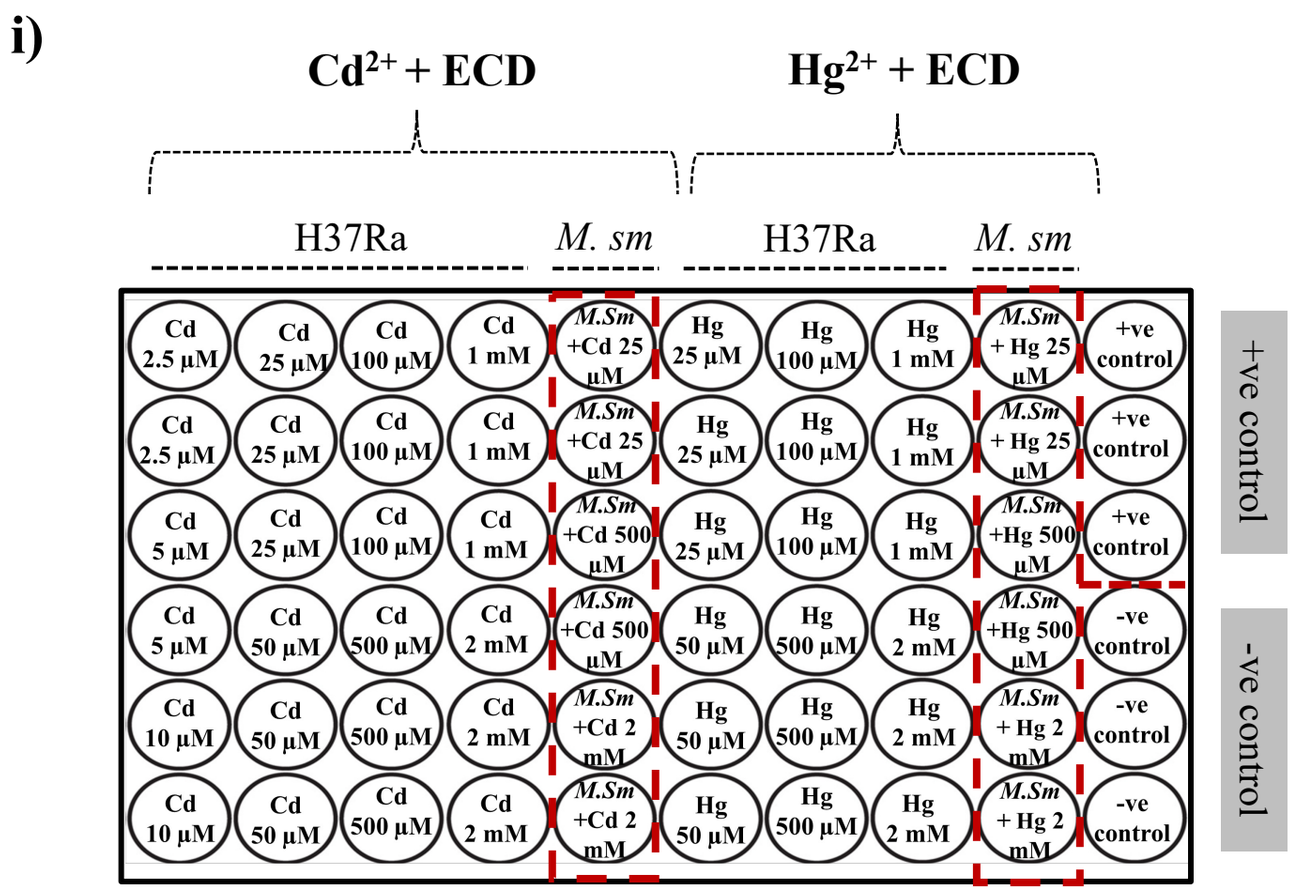
i)
Cd2+ + ECD
Hg2+ + ECD
H37Ra
M. sm
H37Ra
M. sm
Cd 2.5 µM
Cd 25 µM
Cd 100 µM
Cd 1 mM
M.Sm +Cd 25 µM
Hg 25 µM
Hg 100 µM
Hg 1 mM
M.Sm + Hg 25 µM
+ve control
Cd 5 µM
Cd 50 µM
Cd 500 µM
Cd 2 mM
M.Sm +Cd 500 µM
Hg 50 µM
Hg 500 µM
Hg 2 mM
M.Sm +Hg 500 µM
-ve control
Cd 10 µM
M.Sm +Cd 2 mM
M.Sm + Hg 2 mM
+ve control
-ve control

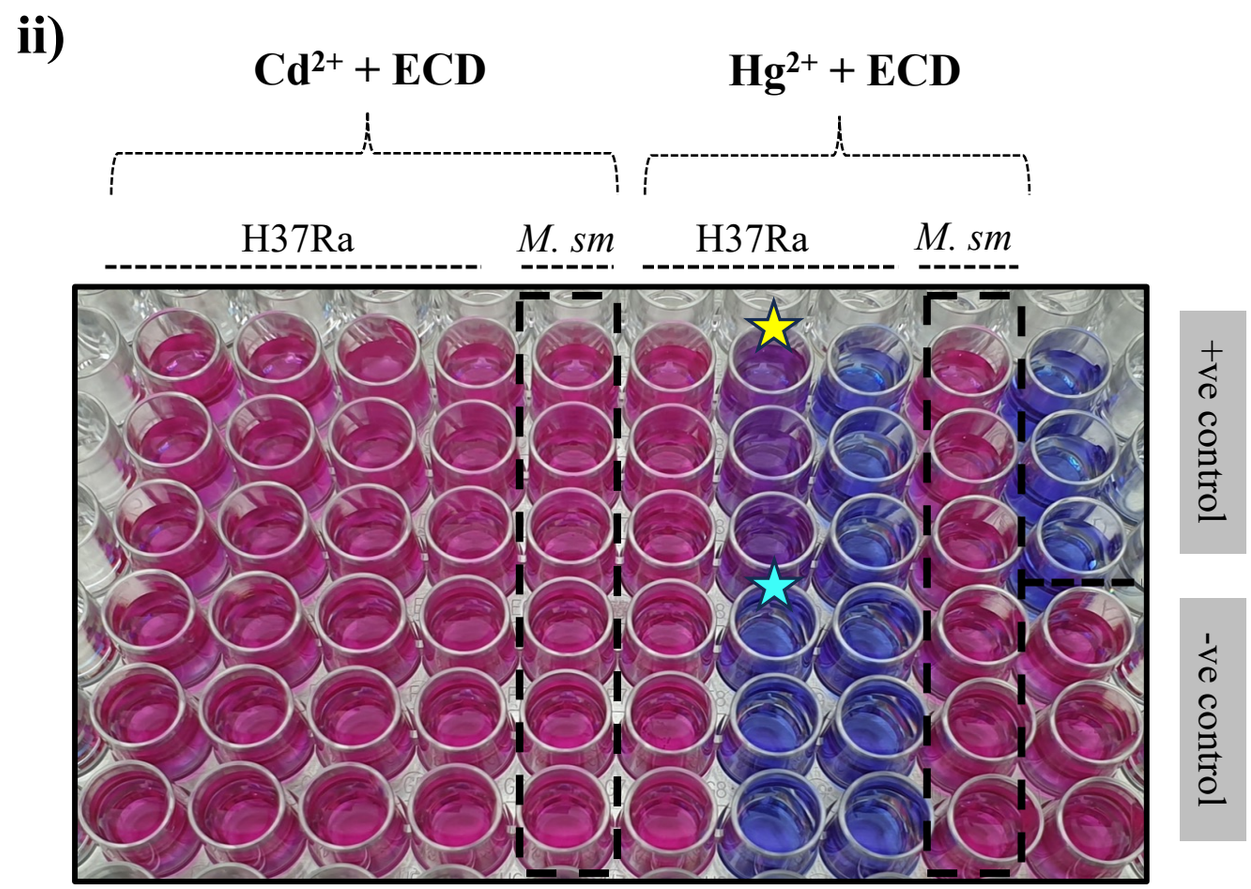
ii)
Cd2+ + ECD
Hg2+ + ECD
H37Ra
M. sm
H37Ra
M. sm
+ve control
-ve control

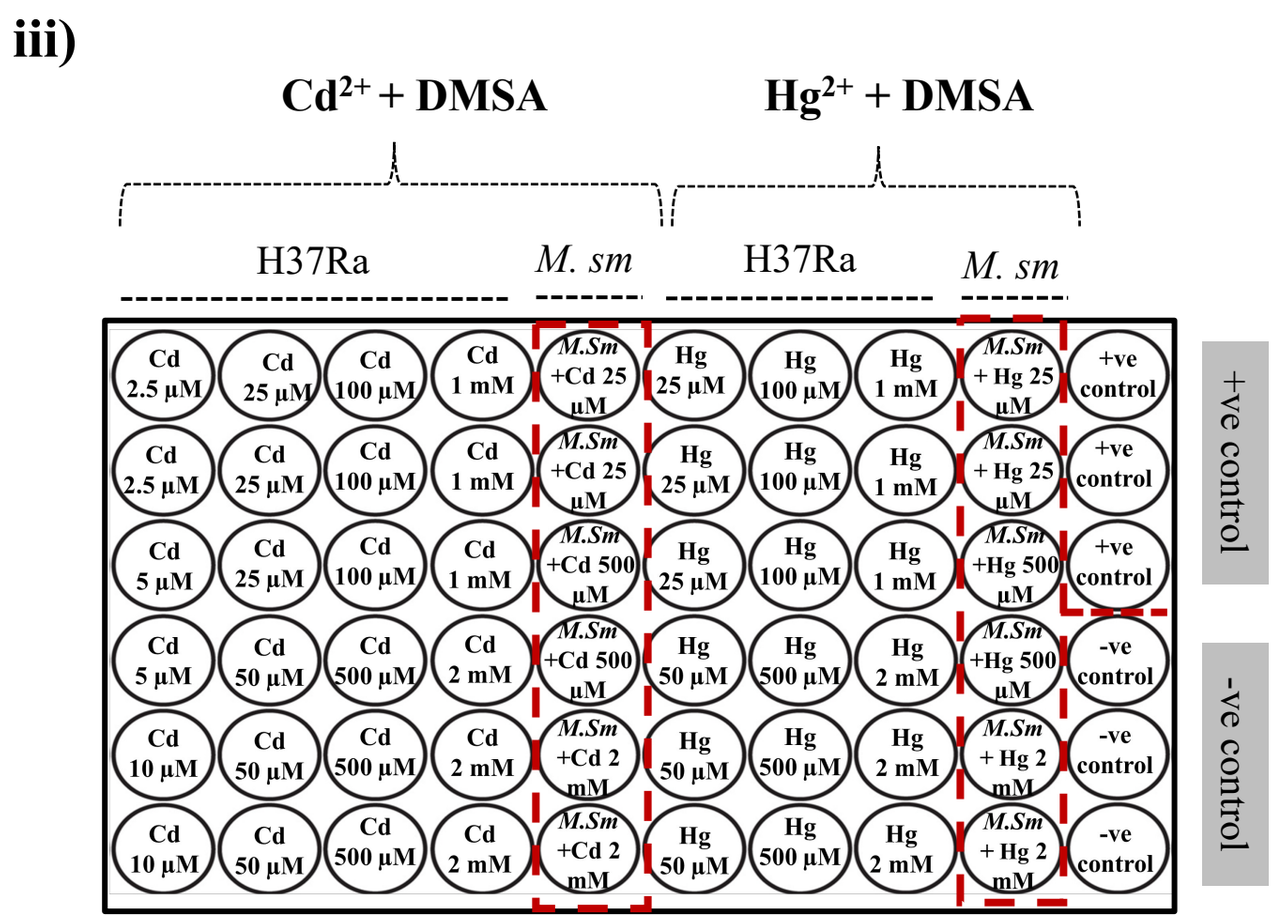
iii)
Cd2+ + DMSA
Hg2+ + DMSA
H37Ra
M. sm
H37Ra
M. sm
Cd 2.5 µM
Cd 25 µM
Cd 100 µM
Cd 1 mM
M.Sm +Cd 25 µM
Hg 25 µM
Hg 100 µM
Hg 1 mM
M.Sm + Hg 25 µM
+ve control
Cd 5 µM
Cd 50 µM
Cd 500 µM
Cd 2 mM
M.Sm +Cd 500 µM
Hg 50 µM
Hg 500 µM
Hg 2 mM
M.Sm +Hg 500 µM
-ve control
Cd 10 µM
M.Sm +Cd 2 mM
M.Sm + Hg 2 mM
+ve control
-ve control

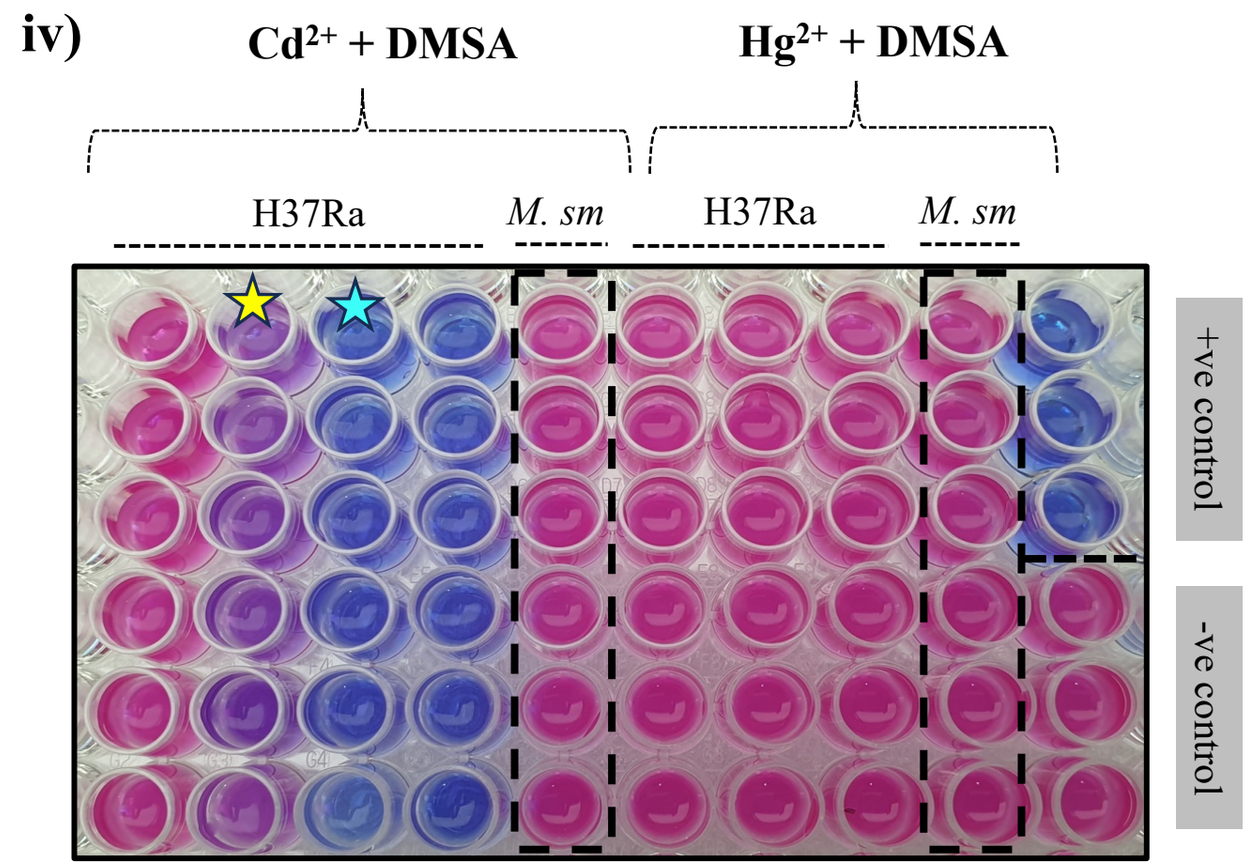
iv)
Cd2+ + DMSA
Hg2+ + DMSA
H37Ra
M. sm
H37Ra
M. sm
+ve control
-ve control

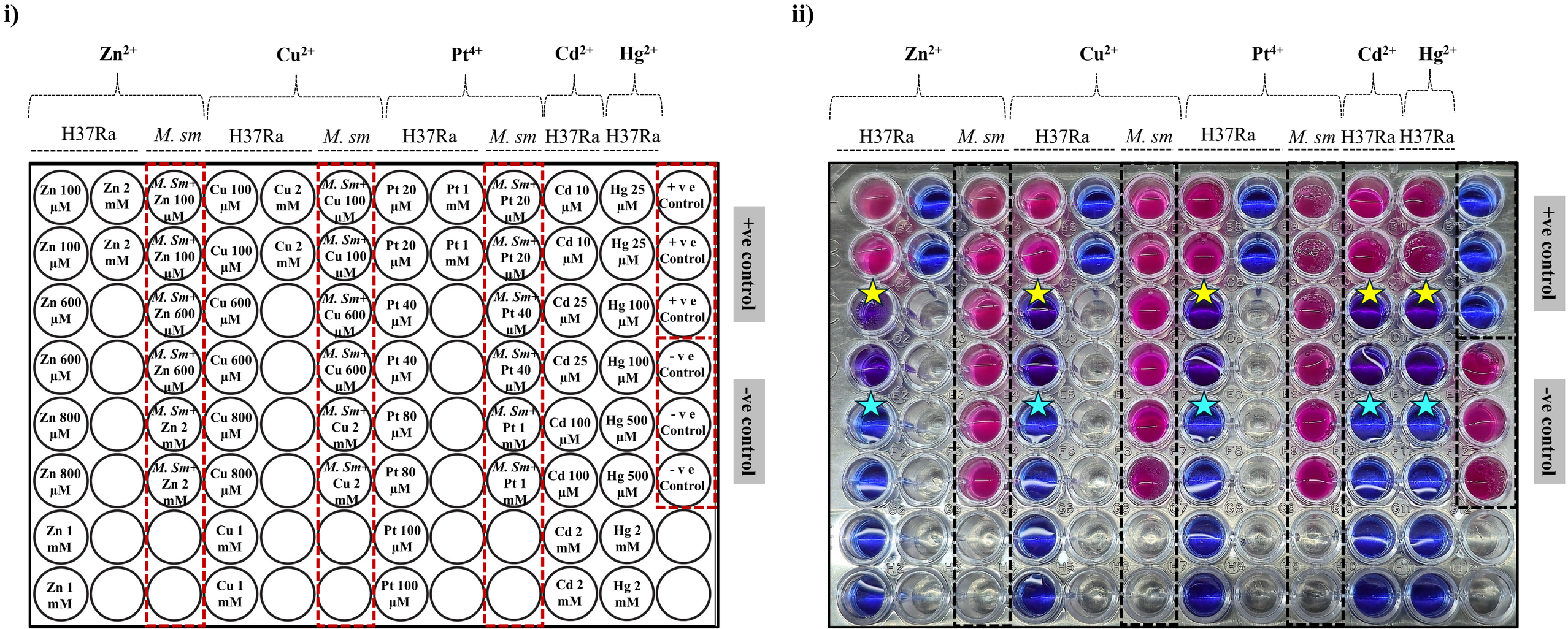
i)
Zn2+
Cu2+
Pt4+
Cd2+
Hg2+
H37Ra
M. sm
H37Ra
M. sm
H37Ra
M. sm
H37Ra
H37Ra
Zn 100 µM
Zn 2 mM
M. Sm+ Zn 100 µM
Cu 100 µM
Cu 2 mM
M. Sm+ Cu 100 µM
Pt 20 µM
Pt 1 mM
M. Sm+ Pt 20 µM
Cd 10 µM
Hg 25 µM
+ v e Control
Zn 100 µM
Zn 2 mM
M. Sm+ Zn 100 µM
Cu 100 µM
Cu 2 mM
M. Sm+ Cu 100 µM
Pt 20 µM
Pt 1 mM
M. Sm+ Pt 20 µM
Cd 10 µM
Hg 25 µM
+ v e Control
Zn 600 µM
M. Sm+ Zn 600 µM
Cu 600 µM
M. Sm+ Cu 600 µM
Pt 40 µM
M. Sm+ Pt 40 µM
Cd 25 µM
Hg 100 µM
+ v e Control
Zn 600 µM
M. Sm+ Zn 600 µM
Cu 600 µM
M. Sm+ Cu 600 µM
Pt 40 µM
M. Sm+ Pt 40 µM
Cd 25 µM
Hg 100 µM
- v e Control
Zn 800 µM
M. Sm+ Zn 2 mM
Cu 800 µM
M. Sm+ Cu 2 mM
Pt 80 µM
M. Sm+ Pt 1 mM
Cd 100 µM
Hg 500 µM
- v e Control
Zn 800 µM
M. Sm+ Zn 2 mM
Cu 800 µM
M. Sm+ Cu 2 mM
Pt 80 µM
M. Sm+ Pt 1 mM
Cd 100 µM
Hg 500 µM
- v e Control
Zn 1 mM
Cu 1 mM
Pt 100 µM
Cd 2 mM
Hg 2 mM
Zn 1 mM
Cu 1 mM
Pt 100 µM
Cd 2 mM
Hg 2 mM
+ve control
-ve control
ii)
Zn2+
Cu2+
Pt4+
Cd2+
Hg2+
H37Ra
M. sm
H37Ra
M. sm
H37Ra
M. sm
H37Ra
H37Ra
+ve control
-ve control

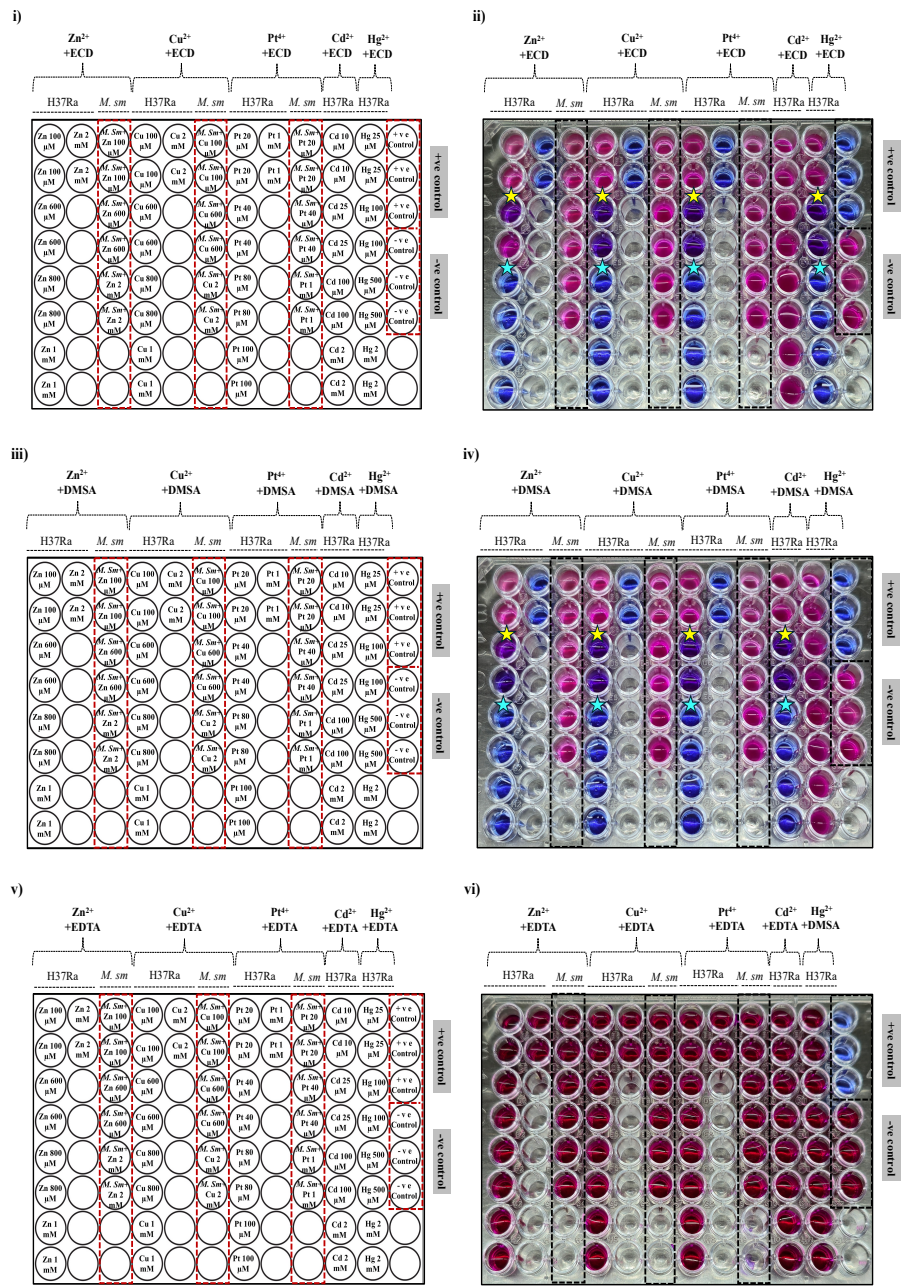
i)
Zn2+ +ECD
Cu2+ +ECD
Pt4+ +ECD
Cd2+ +ECD
Hg2+ +ECD
H37Ra
M. sm
+ve control
-ve control
ii)
iii)
Zn2+ +DMSA
Cu2+ +DMSA
Pt4+ +DMSA
Cd2+ +DMSA
Hg2+ +DMSA
iv)
v)
Zn2+ +EDTA
Cu2+ +EDTA
Pt4+ +EDTA
Cd2+ +EDTA
Hg2+ +EDTA
vi)
Hg2+ +DMSA

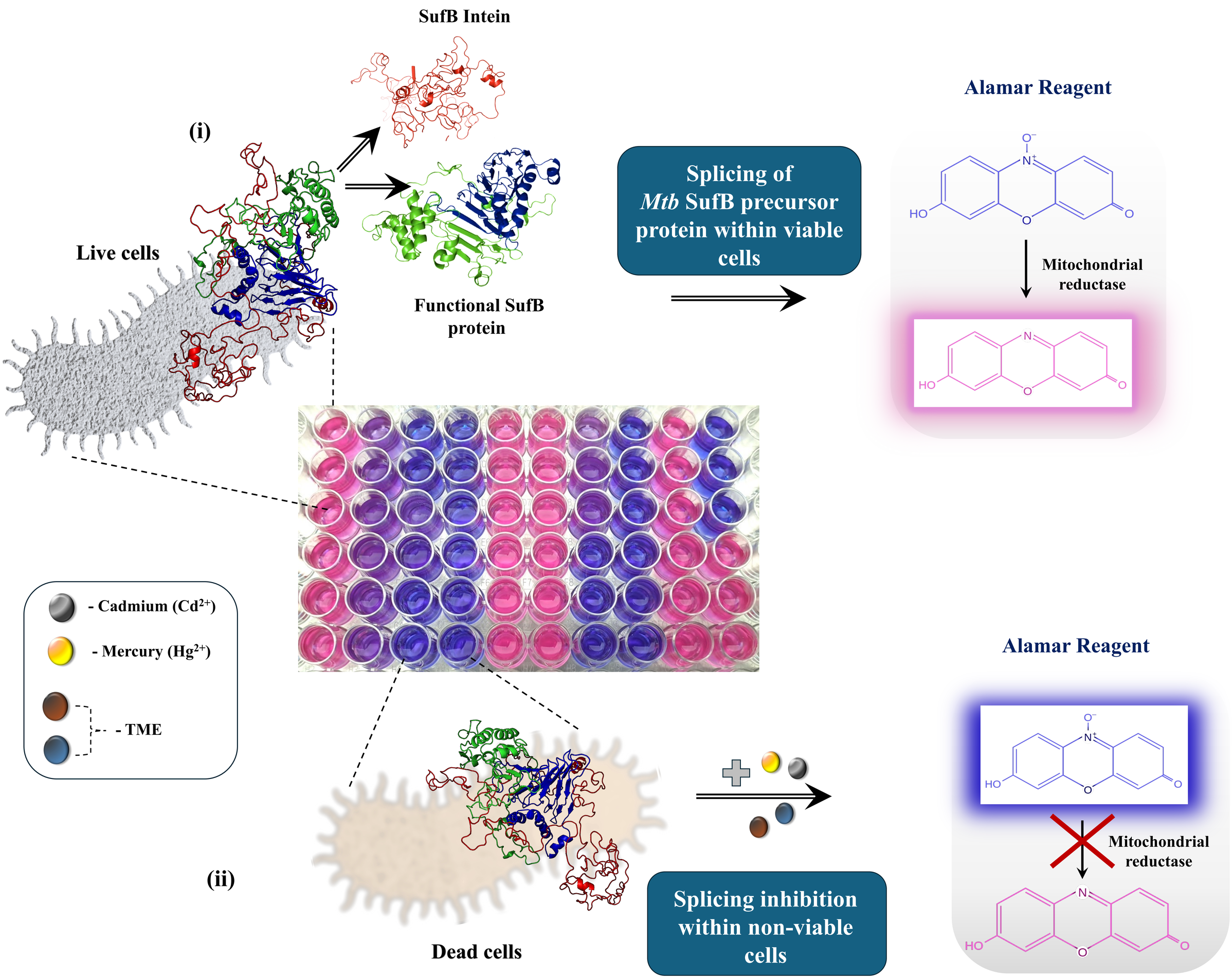
SufB Intein
(i)
Live cells
Functional SufB protein
Splicing of *Mtb* SufB precursor protein within viable cells
Alamar Reagent
Mitochondrial reductase
- Cadmium ($Cd^{2+}$)
- Mercury ($Hg^{2+}$)
- TME
(ii)
Dead cells
Splicing inhibition within non-viable cells
Alamar Reagent
Mitochondrial reductase